Screened Electrostatic Interaction of Charged Colloidal Particles in Nonpolar Liquids

A Thesis
Presented to
The Academic Faculty

by

Carlos Esteban Espinosa

In Partial Fulfillment
of the Requirements for the Degree
Master of Science in Chemical Engineering

School of Chemical & Biomolecular Engineering
Georgia Institute of Technology
August 2010

Screened Electrostatic Interaction of Charged Colloidal Particles in Nonpolar Liquids

Approved by:

Dr. Sven H. Behrens, Adviser
School of Chemical & Biomolecular Engineering
Georgia Institute of Technology

Dr. Victor Breedveld
School of Chemical & Biomolecular Engineering
Georgia Institute of Technology

Dr. Carson Meredith
School of Chemical & Biomolecular Engineering
Georgia Institute of Technology

Date Approved: 12 May 2010

ACKNOWLEDGEMENTS

First, I would like to thank my adviser, Dr. Sven Behrens. His support and orientation was essential throughout the course of this work.

I would like to thank all members of the Behrens group that have made all the difference. Dr. Virendra, a great friend and a fantastic office mate who gave me important feedback and guidance. To Qiong and Adriana who helped me throughout. To Hongzhi Wang, a great office mate.

I would also like to thank Dr. Victor Breedveld and Dr. Carson Meredith for being part of my committee.

Finally I would like to thank those fellow graduate students in the Chemical Engineering Department at Georgia Tech whose friendship I am grateful for.

TABLE OF CONTENTS

LIST OF TABLES

LIST OF FIGURES

SUMMARY

Liquid dispersions of colloidal particles play a big role in nature and as industrial products or intermediates. Their material properties are largely determined by the liquid-mediated particle-particle interaction.

In water-based systems, electric charge is ubiquitous and electrostatic particle interaction often is the primary factor in stabilizing dispersions against decomposition by aggregation and sedimentation. Very nonpolar liquids, by contrast, are usually considered free of charge, because their low dielectric constant raises the electrostatic cost of separating opposite charges above the available thermal energy. Defying this conventional wisdom, nonpolar solutions of certain ionic surfactants do support mobile ions and surface charges. Even some nonionic surfactants have recently been found to raise the conductivity of nonpolar oils and promote surface charging of suspended particles, but this counter-intuitive behavior is not yet widely acknowledged, nor is the mechanism of charging understood.

The present study provides the first characterization of the electrostatic particle interaction caused by nonionizable surfactants in nonpolar oils. The methods used in this study are video microscopy experiments where particle positions of equilibrium ensembles are obtained and translated into particle interactions.

Experimentally, equilibrium particle positions are monitored by digital video microscopy, and subjected to liquid structure analysis in order to find the energy of interaction between two particles. The observed interaction energy profiles agree well with a screened-Coulomb potential, thus confirming the presence of both surface charge and mobile ions in solution. In contrast to recently reported electrostatic

particle interactions induced by ionic surfactants in nonpolar solution, the present study finds evidence of charge screening both above and below the surfactant's critical micelle concentration, CMC. Fitted Debye screening lengths are much larger than in aqueous systems, but similar to the Debye length in nonpolar oils reported for micellar solutions of ionic surfactants [1].

Radial distribution functions obtained from experiments are compared to Monte-Carlo simulations with input potentials obtained from a fit to the interaction measurement. The measured electrostatic forces and fitted surface potentials are fairly substantial and easily capable of stabilizing colloidal dispersions. Although few in number, surface charges formed on polymer particle surfaces submerged in nonpolar solutions of nonionizable surfactants create surface potentials comparable to those in aqueous systems.

CHAPTER I

INTRODUCTION

The fundamental understanding of particle interactions in liquid media is necessary to understand phenomena for practical applications in biological systems and industry. Living organisms are based on cells, units of complex lifeforms full of colloidal interactions both inside a cellular aqueous core and at the cellar interfaces. In the oil industry, novel and useful techniques exploit particle behavior at liquid-liquid interfaces as part of oil extraction techniques and is also used to remove natural particulates from oil mixtures [2].

The understanding of particle interactions is used to control particle self-assembly into structures for photonic applications [3] or drug delivery [4]. Pieranski successfully created two-dimensional crystal monolayers by placing carefully selected polymer particles on a water and air interface [5]. Hollow spheres can be made by the controlled self-assembly of colloidal spherical particles on the surface of emulsion droplets, with subsequent steps used to remove the disperse phased and create the hollow assembled structures [6].

Electrostatic interactions in aqueous systems are ubiquitous and the topic is sufficiently investigated to the point that few questions remain unanswered in the field. The formation of ions in an aqueous environment is easily achieved with thermal energy at standard conditions readily exceeding the energetic cost of separating opposite charges. With ion dissociation being a favorable process in aqueous systems, controlling the amount of ions in solutions becomes a simple matter of varying concentration of salt. Similarly, particle surfaces readily acquire electric charge by dissociation of ionizable functional surface groups or by adsorption of ionic species from solution.

In nonpolar media, characterized by low dielectric constants ($\varepsilon < 5$), however, the presence of charge and the interaction between charges is surprising and poorly understood. Theory would predict that the separation of charges in nonpolar liquids is insignificant because of the large energy of ion association in such low dielectric constant media.

Yet, contrary to common knowledge, strong charge effects are experimentally observed in nonpolar solutions of ionizable surfactants [7]. Some surfactants with ionic groups have been shown to readily increase the conductivity of nonpolar solvents [8, 9] and increase the surface charge of immersed solid particles [10, 11, 12].

The mechanisms by which these surfactants induce both charge formation in solution and surface charging are unknown. Ionic surfactants at concentrations above the critical micelle concentration, CMC, in nonpolar solvents form inverse micelles which seem to be able, according to a recent hypothesis, to disproportionate, a process by which two neutral bodies react into a pair of oppositely-charged, separate bodies [13, 14]. Experiments have shown that conductivity increases, however, occur at concentrations both above and below ionic surfactant's CMC in nonpolar oils [1, 13]. A very recent hypothesis suggests that nonpolar solutions of ionizable surfactant above the CMC, undergo micelle disproportionation to form charges, whereas below the CMC, the dissociation of individual surfactant molecules is responsible for charge formation [9].

A recent study by Dukhin and Goetz surprisingly showed how several nonpolar solutions of nonionizable surfactants can introduce mobile charge and sustain particle surface charge in nonpolar solvents, as observed through conductivity increases with rising surfactant concentration [15]. Another study further investigated the conductivity of nonpolar solutions of nonionizable surfactants and found evidence for charge disproportionation both above and below the CMC; micelle disproportionation into oppositely charged micelles is the charging mechanism [16]. This in contrast to ionic

surfactant systems where dissociation is the hypothesized charging mechanism below the CMC. Evidence for surface charging of particles suspended in nonpolar solutions of nonionic surfactant has also been found below the CMC [17]. The existence of surface charges and mobile ions in solution should manifest itself in the solution-mediated particle interaction, but so far interaction measurements in nonpolar solutions of nonionizable surfactants have not yet been performed.

Such interaction measurements are the subject of this study. Particle interaction energy profiles are extracted for equilibrium particle positions observed by digital video microscopy. Fitted theoretical interaction profiles are used as input for Monte-Carlo simulations of the dispersion's liquid structure. Comparison with theoretical energy profiles are carried out both directly and at the level of the observed particle configurations using Monte-Carlo simulations. The goal is to test whether the interaction induced by nonionizable surfactants in nonpolar dispersions is indeed electrostatic, and if so, to obtain information about the particle charges and ion content of the solution that may ultimately provide a better understanding of the underlying charging mechanism.

CHAPTER II

BACKGROUND

2.1 Electrostatics in nonpolar fluids

2.1.1 Charge formation in nonpolar fluids

In this study, the charging phenomena of nonpolar liquids using nonionizable surfactants is observed by analyzing how polymer particles interact in such media. A polar liquid is reflected by its ability to separate charge within its molecule in order to induce a a dipole moment, more generally a multipole moment. Polarization is caused by electronegativity differences between a molecule's atoms and structural asymmetry of the molecule. The consequence of polar molecules is that strong intermolecular multipole and induced multipole forces have a strong influence on physical processes such as phase transition temperatures, fluid surface tension, solubility of solutes, and the solubility of ions.

A solvent's polarity is quantified by its dielectric constant, ε, the ratio of the permittivity of charge when a voltage is applied across a medium relative to the permittivity of charge in a vacuum; in essence a liquid's ability to solubilize ions. Solvents can be categorized to be in a range of polarity as polar, $\varepsilon > 11$, where substantial ion-solvation is possible, low polar, $5 \leq \varepsilon \leq 11$, where ion solvation is relatively poor and electrostatic effects are rare, to non-polar, $\varepsilon < 5$, where conventional theory would predict that ion solvation is low enough to safely assume it does not exist [18].

In order to quantify a solvent's ion solubility, one can begin by looking at what is the energetic barrier that needs to be overcome in order for ions to dissociate. The energetic quantity that determines how strongly bound two ions are is the Coulomb energy, which for a pair-of ions of charge Z_1 and Z_2 is:

$$E_{Coulomb} = \frac{(Z_1 e)(Z_2 e)}{4\pi\varepsilon\varepsilon_0 r_{12}} \tag{1}$$

where (Ze) is the charge of each ion as a product of the valency Z with the elementary charge e, ε_0 is the permittivity of a vacuum and r_{12} is the separation between the ions.

Statistical mechanical theory states that the probability of ion formation in any solvent is proportional to the exponential of the Boltzmann factor of the Coulombic energy:

$$exp\left(\frac{E_{Coulomb}}{k_B T}\right) \tag{2}$$

where $k_B T$ is the available thermal energy with k being the Boltzmann constant, $1.38 \cdot 10^{-23} J/K$, and T is the absolute temperature. Note that for a pair of opposite charged ions, such as a salt, the product $(Z_1 e)(Z_2 e)$ is negative and the probability of dissociation exponentially decreases with increasing valencies Z_1 and Z_2. The ratio of the Coulomb energy relative to the thermal energy is commonly referred to as a ratio of appropriate length scales as:

$$\frac{E_{Coulomb}}{k_B T} = \frac{-\lambda_B}{r_{12}} \tag{3}$$

where λ_B is the Bjerrum length defined to be the distance at which the Coulombic energy of a pair of oppositely-charged elementary ions equals in magnitude to the available thermal energy; a property of the liquid.

$$\lambda_B = \frac{e^2}{4\pi\varepsilon\varepsilon_o k_B T} \tag{4}$$

The usefulness in defining the Boltzmann factor of the Coulomb energy as a ratio of length scales is that one can look at the problem of ion dissociation in two separate yet equivalent statements that relate energetic barriers and length barriers against

dissociation. In energetic terms, if the thermal energy is large enough to overcome the Coulombic energy between ions, dissociation is favorable. Similarly, in length scales, if the distance of closest approach of a pair of ions, which depend on the size of the ions: $r_{12min} = R_1 + R_2$, is large enough relative to a solvent's Bjerrum length, then the probability of ion formation is large.

In aqueous systems, $\varepsilon = 80$, it is well known that salt readily dissociates as the large dielectric constant translates into a low Bjerrum length of 0.7 nm. However, a salt such as NaCl has a crystal length of 0.28 nm, with similar common salts being in similar length scales, which means merely ion size would not be enough to surpass the Bjerrum length. But, a characteristic of ion solvation in water is that due to water's strong dipole moment and strong affinity for ions, tightly packed layers of water molecules stick to ion surfaces, effectively encasing bare ions. The sum of the size of ions and bound water layers increases the distance of closest approach between ions making it larger than the Bjerrum length; consequently dissociation is strongly favorable in aqueous systems [7].

However, in nonpolar systems, $\varepsilon \simeq 2$, the Coulombic energy is 40 times larger due to the dielectric constant difference relative to water. Consequently, the Bjerrum length is 40 times larger as well at 28 nm. In order for ions to dissociate in water, the size of the ions in nonpolar oils should be at least 14 nm in length, far larger than the size of any common salt. Herein lies the quantifiable reason for statements in current statistical mechanical theory that make the assumption that the dissociation of ions in nonpolar solutions is effectively non-existent.

2.1.2 Charge formation in nonpolar oils with ionic surfactants

It has been established that ions need to be large enough in order to dissociate in solution. In order to overcome the energetic barrier of separating opposite charges in a nonpolar fluid, one can look at finding aggregate, ionizable structures that meet

the length scale of the Bjerrum length, such as ionic surfactant micelles. Surfactant micelles, in charge-hostile environments such as nonpolar oils, can be thought of as being giant salt ions capable of introducing charge were there should be none. Experiments have shown that increases the concentration of of ionic surfactants in nonpolar oils increases the charge conductivity of the media [7]. One of the most studied ionic surfactants is Aerosol-OT (AOT), di-(2-ethylhexyl) sodium sulfosuccinate (See Figure 1). AOT is a versatile component due to its ability to dissolve and to form micelles in solvents in the range of polarity between water ($\varepsilon = 80$) to oils ($\varepsilon = 2$) [19].

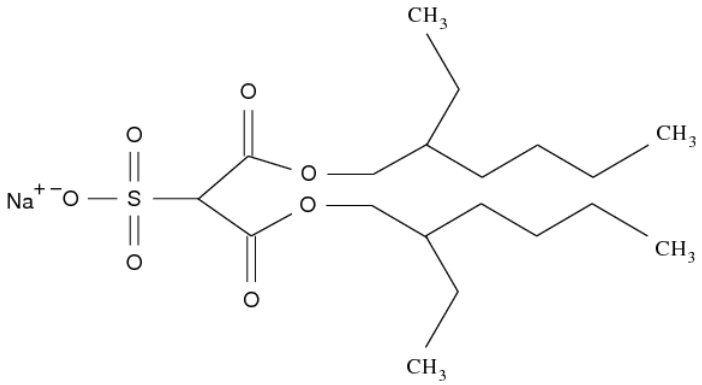

Figure 1: Chemical structure of Aerosol-OT, trade name for di-(2-ethylhexyl) sodium sulfosuccinate

Some surfactants with ionic groups have been shown to readily increase the conductivity of nonpolar solvents [8, 9]. Also, nonpolar solutions of ionic surfactants increase the surface charge of immersed solid particles [10, 11, 12]. The mechanisms by which these surfactants induce both charge formation in solution and surface charges are unknown. A recent hypothesis is that ionic surfactants at concentrations above the critical micelle concentration, CMC, in nonpolar solvents form inverse micelles which disproportionate, a process by which two neutral micelles react into a pair of oppositely separate charged micelles [13, 14]. A disproportionation of two micelles, can be symbolically represented as $2M \longleftrightarrow M^+ + M^-$; in contrast to a dissociation which can be represented for an arbitrary compound, AB, as: $AB \longleftrightarrow A^+ + B^-$

Experiments have shown that conductivity increases, however, occur at concentrations both above and below ionic surfactant's CMC in nonpolar oils [1, 13]. A very recent hypothesis suggests that nonpolar solutions of ionizable surfactant above the CMC, undergo micelle disproportionation to form charges; while below the CMC, dissociation of independent surfactant molecules forms charges in solution [9].

2.1.3 Charge formation in nonpolar solutions of nonionizable surfactants

So far it has been shown that an ionic, dissociable surfactant, such as AOT, is able to provide large enough ions in nonpolar media to allow for the occurrence of charge. Unconventional results show that non-ionic surfactants in nonpolar fluids increase the electrical conductivity, supporting the claim that charges can be present in said nonpolar solutions. In particular, surfactants in the Span family have shown surprisingly high conductivities despite of the fact that none of their functional groups is ionic or dissociable [15]. Increasing concentrations of these surfactants in a range of nonpolar fluids($(\varepsilon = 3$ to $\varepsilon = 8)$ increases the conductivity substantially, see Figure 2.

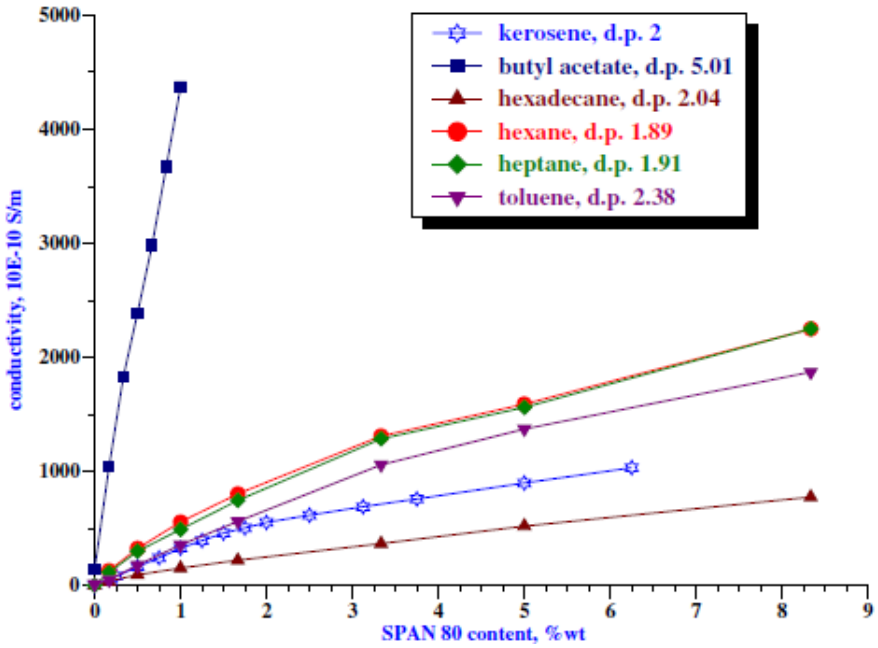

Figure 2: Conductivity of various nonpolar liquids with Span 80 obtained from [Dukhin and Goetz, 2006]. Abbreviation d.p = dielectric permittivity

Figure 2 shows how butyl acetate ($\varepsilon = 5.01$) shows the steepest increase in conductivity with varying concentration of surfactant. The next most responsive fluid in conductivity effects is Hexane ($\varepsilon = 1.89$), the most nonpolar of all solvents assessed. The surfactant used in Figure 2 is Sorbitan mono-oleate, tradename Span 80 whose chemical structure is shown in Figure 3.

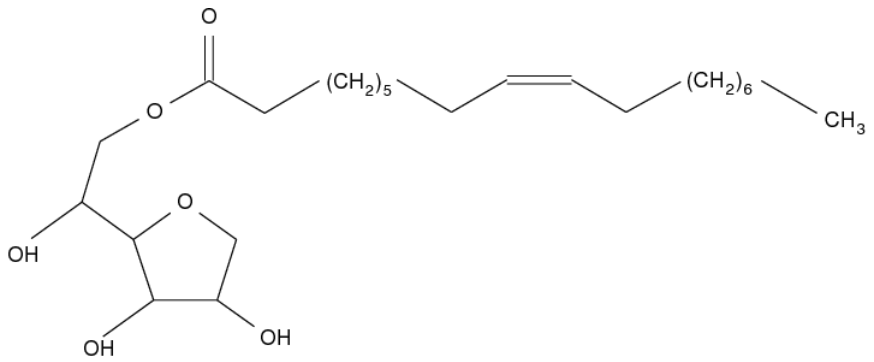

Figure 3: Chemical structure of Sodium mono-oleate, tradename Span 80

In Span 80 there is no dissociable group, as can be seen in Figure 3, in strong contrast to AOT which is ionic. Guo reports that Sorbitan trioleate surfactant (Span 85) in Hexane exhibits two distinct conductivity regimes above and below the CMC [16], see Figure 4. Yet, one conclusion supported by their data is that disproportionation takes place above and below the CMC; in contrast to AOT where experiments report disproportionation forms charges above the CMC, yet dissociation below the CMC [9].

Similarly, very recent electrophoretic mobility experiments reveal that the acquisition of surface charge on submerged polymer particles in nonpolar solutions of nonionizable surfactants occurs both above and below the CMC of the surfactant [17]. As seen in Figure 5, the surface potential is quantified by the so called $\zeta - potential$ known as the electrostatic potential at the hydrodynamic slipping plane close to a surface. The true surface potential, Ψ_0 is a quantity that cannot be experimentally measured, in contrast to the ζ-potential which is directly related to the mesasurable electrophoretic mobility; but, for nonpolar fluids theory shows that $\Psi_0 \approx \zeta$ [20]

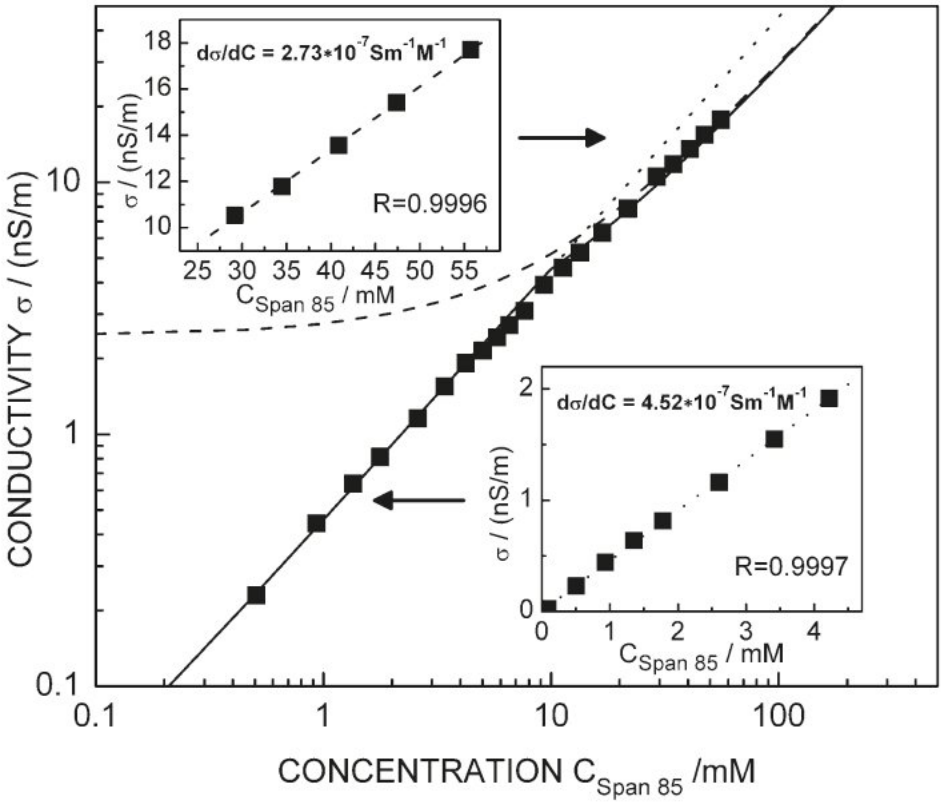

Figure 4: Conductivity of Hexane with added Span 85 by [Guo, 2009]: "markers, experimental data; dashed line, linear fit (with additive offset) for the micelle-dominated regime; dotted line, linear fit for the submicellar regime; solid line, double linear fit described in the text. Insets: linear portions above and below the critical micelle concentration."

Particularly, it can be seen in Figure 5 that at low surfactant concentrations, the ζ-potential is largest, indicative of the largest sampled surface charge. The implications of these studies is that particle interactions in nonpolar solutions of nonionizable surfactants will manifest evidence that indeed mobile ions and surface charge occur.

2.1.4 Electrostatic particle interactions

Electrostatic stabilization has been reserved in the past for aqueous solutions as electrostatic effects were thought of to exclusively occur in aqueous or polar systems. To analyze the effects of electrostatics in oils, the theory behind aqueous charge-stabilized colloidal dispersions will be briefly reviewed. When charge is able to reside

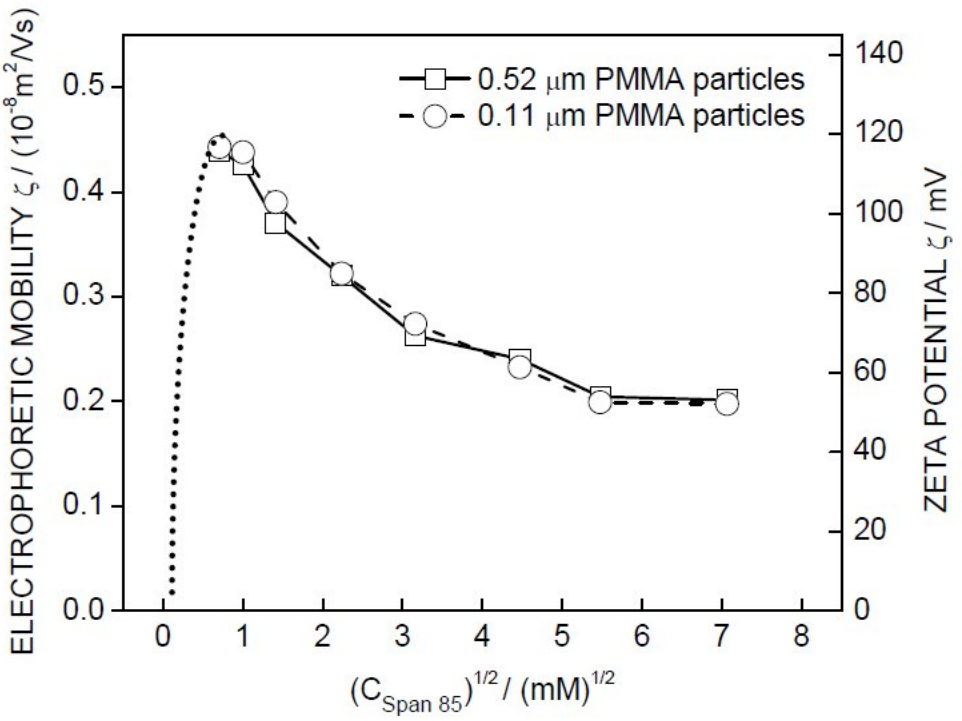

Figure 5: Data obtained from [Espinosa, to be published]. Electrophoretic mobility and zeta potential of PMMA particles as a function of the square root of the Span 85 concentration in Hexane. Square markers and solid line for the 0.52 μm diameter particles; circle markers and dash line for the 0.11 μm diameter particles; dot line for the conceptual way of charging up the particles.

on a particle surface, a particle dispersion can be stabilized against aggregation by exploiting the repulsive interactions and can be described by the theory of Derjaguin Landau Verwey and Overbeek (DLVO)[21, 22]. DLVO theory is important as it will be applied to a system it is rarely related to in this work, nonpolar fluids.

DLVO theory states that charged-stabilized colloidal interactions are dominated by electrostatic repulsions and Van der Waals dispersion attractions. DLVO theory is particularly well known to work in systems were colloidal surfaces contain dissociable chemical groups. The charges at the surface and the counter ions in solution form a so called electric double layer. Hence the electrostatic repulsion is called a double-layer repulsion. The range of interaction of the double-layer repulsion is characterized by the Debye length, κ^{-1}.

$$\kappa^{-1} = \sqrt{\left(\frac{\varepsilon\varepsilon_o k_B T}{\sum_i \rho_{\infty i} e^2 z_i^2}\right)} \tag{5}$$

Where $\rho_{\infty i}$ is the concentration of ions in the bulk fluid far away from the surface. The Debye length is inversely proportional to the concentration of ions in solution. The larger the concentration of ions in solution reflect a small κ^{-1} as a larger amount of ions effectively "screen" the interaction.

The Debye length is the characteristic length scale based on the Debye-Huckel equation, which is a linearized Poisson-Boltzmann equation, describing the behavior of the electrostatic potential, Ψ, in an electrolyte solution [23]:

$$\bigtriangledown^2 \Psi = \kappa^2 \Psi \tag{6}$$

where Ψ is written in non-dimensional form: $\Psi = \frac{e_0 \psi}{k_B T}$, e_0 being the elementary charge and $k_B T$ the thermal energy. For the simplest case, this theory can be used to compute the decay in the potential of a charged planar surface in an electrolyte solution as shown in Figure 6.

The Debye length, defined by Eq. 5, can be interpreted as the characteristic length over which the electrostatic potential decays with distance from the surface, as seen in the lower plots in Figure 6. The significance of the Stern layer, shown in Figure 6 as a dotted line near the surfaces, is that ions in solution have a finite particle size; the decay in the potential begins where ions are freely mobile, not perfectly at the surface of a charged material, but a distance δ away from the surface. The decay of the electrostatic potential radially extending from a particle with surface charge Z_1 and radius, $R_{particle}$, can be described by a Debye-Huckel equation in spherical coordinates:

$$\bigtriangledown^2 \Psi = \frac{1}{r^2}\frac{d}{dr}\left(r^2 \frac{d\Psi}{dr}\right) = \kappa^2 \Psi \tag{7}$$

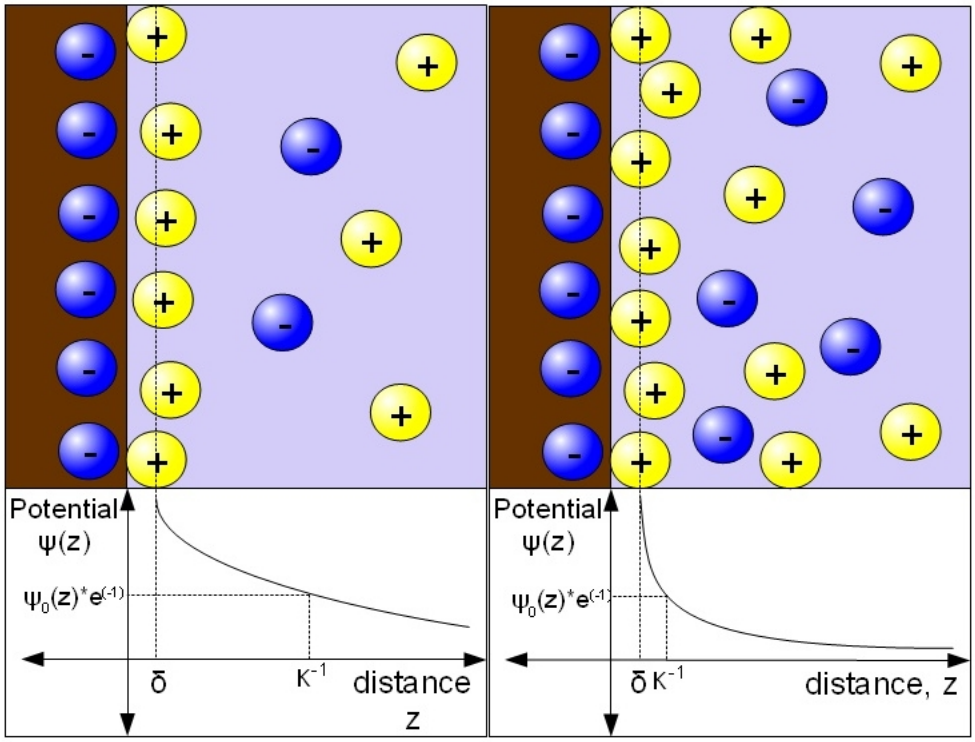

Figure 6: Planar charged surface in an electrolyte solution illustrating the effect of ion concentration, quantified by the Debye length, κ^{-1}, on the decay of the potential, Ψ, starting from a stern layer δ. (Left) Negatively-charged surface on a low ion concentration solution with relatively large κ^{-1}. (Right) Negatively-charged surface in a high ion concentration solution with a relatively short κ^{-1}

Using two boundary conditions based on the information that the potential decays to zero for infinite separations,

$$\Psi(r \to \infty) = 0 \tag{8}$$

while at the surface of the ion, the gradient of the interaction is proportional to the charge density at the surface as determined by Gauss' Law:

$$-\varepsilon\varepsilon_0 \frac{d\Psi}{dr}\Big|_{r=R_{particle}} = \frac{-(Z*e)}{4\pi R^2_{particle}} \tag{9}$$

gives the electrostatic potential of the particle in an electrolyte medium as a function of the radial distance.

$$\Psi(r) = \frac{(Z_1^* e)}{(4\pi\varepsilon\varepsilon_0)\, r} \frac{exp(\kappa R_{particle})}{1 + \kappa R_{particle}} exp(-\kappa r) \tag{10}$$

The pair-interaction, u(r), that two equally-charged particles feel between each other can be obtained by looking at the potential that the second particle with charge, Z^*e experiences due to the the electrostatic potential of the first, Ψ as:

$$u(r) = \Psi(r) \cdot (Z^*e) \cdot \frac{exp(\kappa R_{particle})}{1 + \kappa R_{particle}} \tag{11}$$

which forms the well-known screened-Coulomb interaction potential:

$$u(r) = \underbrace{\frac{(Z^*e)^2}{(4\pi\varepsilon\varepsilon_0)\, r}}_{\text{Coulomb term}} \underbrace{\frac{exp(2\kappa R_{particle})}{(1 + \kappa R_{particle})^2}}_{\text{Finite particle size}} \underbrace{exp(-\kappa r)}_{\text{Screening}} \tag{12}$$

The significance of an effective charge number is non-trivial. Non-linear charge dissociations near the particle's surface make it near impossible to measure experimentally the fully dissociated surface charge, Z. What is measured experimentally is the effective charge number, Z*, which can be up to 2 orders of magnitude smaller than Z in aqueous systems [24].

The DLVO, as mentioned, is dominant in aqueous dispersions where charge at a surface and mobile ions are readily available and a screened-Coulomb describes particle interactions well. Recent evidence of surface charge and charge formation in nonpolar solutions of nonionizable surfactants would be elucidated by particle interactions in the framework of screened-Coulomb interactions.

CHAPTER III

METHODS

3.1 Video microscopy

The information about interaction energy (and forces) is contained in equilibrium structure of particle ensembles were the spatial arrangement of said particles can be characterized. In this study, particle interactions are analyzed by observing and processing microscopy images of particle ensembles in a 2-dimensional setting. A broad description of the video microscopy procedure will be developed.

In order to analyze images, a video microscopy method described by Crocker and Grier [25] is used as a starting point together with the development of viewing cells that locate particles in 2-dimensions pioneered by Park et Al. and shown in Figure 7 [26].

The setup, as seen in Figure 7, consists of a glass cell were particles to be analyzed are confined in a 2-dimensional plane. An inverted microscope then focuses at the cell from underneath. The microscope consists of the objective connected to a charged-coupled detector (CCD) which then feeds the output signal into a computer to record the images. The device in question is a *Nikon Eclipse TE2000-E* inverted optical microscope.

3.2 Image processing

In order to analyze the spatial equilibrium configurations, images are then processed into particle positions accurately using publicly available routines in MATLAB. In order to be able to accurately locate the particles, published programs are used to clear background noise from the image, locate particle peaks and calculate the centroids

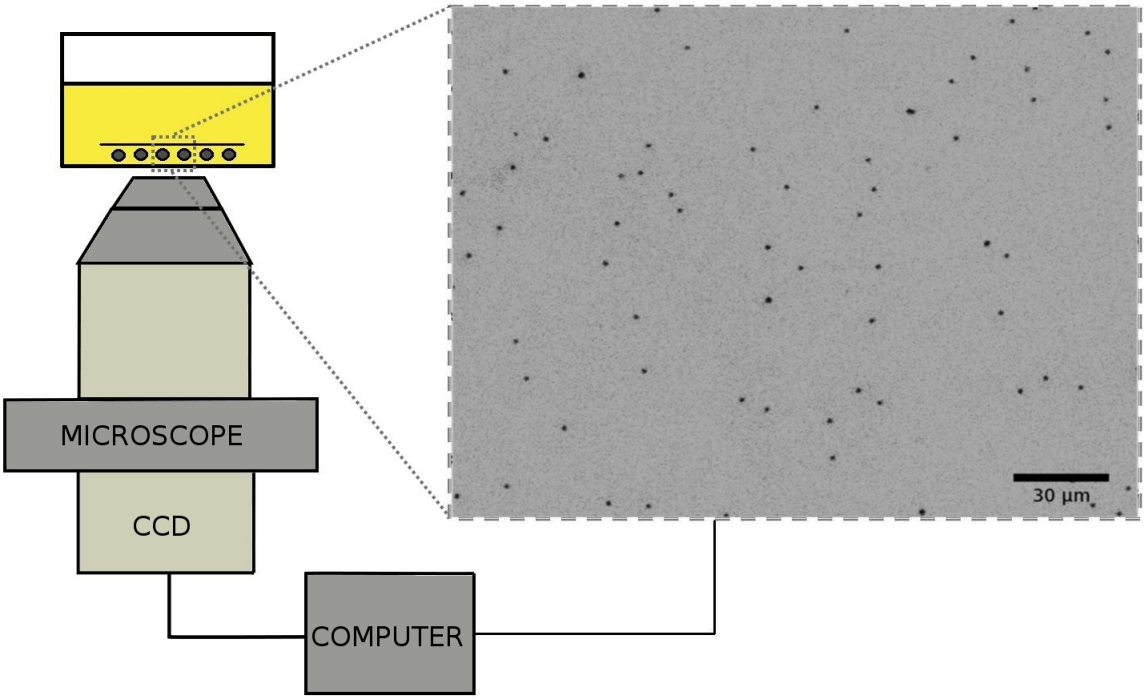

Figure 7: Overall video microscopy setup for a general 2-D dispersion viewing cell. The image of the 2-D dispersion was obtained experimentally (Based on experimental setup by [Park, 2008] and [Crocker, 1996])

of the regions of interest, the particles. Crocker & Grier created a set of programs which have been extensively tested and improved with time and made them publicly available; the details behind such programs can be found on reports by the authors [25]. An overview of how these programs work and how they are embedded into programs developed in this project are briefly described.

3.2.1 Particle positions

Movies of 2-D dispersions are exported using Nikon's software **NIS Elements 3.0** into a series of "tiff" formatted images. Such image format can be readily processed in

MATLAB. The first step is to import the image into MATLAB using the Image Acquisition Toolbox. With the import function, raw gray scale tiff images are translated into matrices containing indexes to represent the gray scale value for each pixel.

In order to locate particle positions, the background has to be distinguished from the particles. First a bandpass program is called to remove the background through a series of convolutions to average out the background in order to remain with particles only. Another program finds the peaks in the remaining elements or particles above a certain user-defined threshold. Then, a program is called to find the centroid representing the peaks of the particles in the image. The centroid finder is necessary as note that intensity peaks don't necessarily correspond to a particle center, and so this program finds that center accurately.

3.3 Radial distribution function

With particle positions being reliably accessible, the next step is to process them and obtain statistical mechanical quantities that will be further processed into pair interactions. Before describing the methods that translate spatial arrangements of particle ensembles into interaction potentials, the definition and computation of quantities that describe ensembles is first discussed. The quantity used in this study for the purpose of describing particle ensembles is the radial distribution function, g(r). The radial distribution function of an ensemble is the probability of finding a particle a distance (r) away from a reference particle. The g(r) is a statistical measure of the structure of an ensemble being analyzed.

In 2-D systems, such as those represented in this work, in order to calculate a radial distribution function, a reference particle is chosen as shown in Figure 8. From that reference particle, the number of particles, n, that fall within a shell of radius r and $r + \delta r$ are counted and quantified into a distribution by normalizing relative to the number density of particles in the whole state, $\rho_{total} = N_{frame}/A_{frame}$:

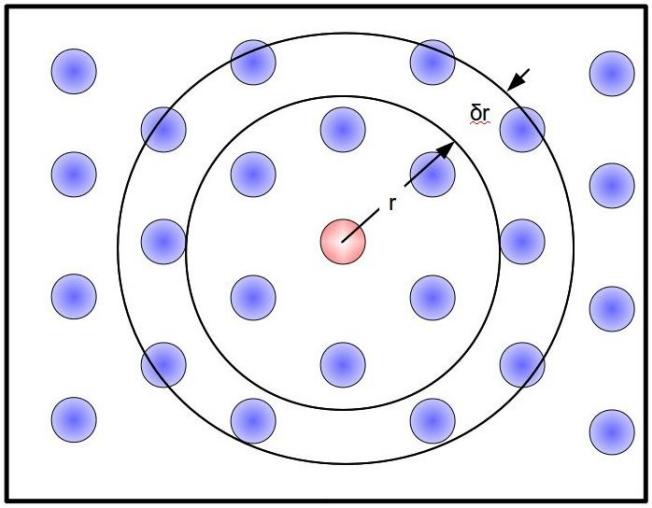

Figure 8: Description of getting a radial distribution function, g(r), of a typical colloidal dispersion

$$g(r) = \frac{\rho_{local}(r)}{\bar{\rho}_{total}} = \frac{n(r)}{A_{shell} \cdot \bar{\rho}_{total}} \tag{13}$$

The area of the shell is $A_{shell} = \pi((r + \delta r)^2 - r^2) = 2\pi r\delta r + \pi\delta r^2$, consequently the radial distribution function for each shell is:

$$g(r) = \frac{n(r)}{(2\pi r\delta r + \pi\delta r^2) \cdot \rho_{total}} \tag{14}$$

In order to get a distribution for the entire frame, g(r)'s are obtained for shells at many bins up to an arbitrary maximum separation. The maximum distance sampled is adequate in dispersion science once all the features of the distribution function are captured and it is observed that at large separations the distribution converges to unity.

An important distinction that needs to be made is that the g(r) is sensitive to the particle concentration of an ensemble. This is in contrast to other measures such as a pair-potential which is independent of particle concentration. Consequently, the radial distribution function is not unique to the same system (the solid surfaces and the media are the same) if the number density changes. Figure 9 describes this

difference graphically.

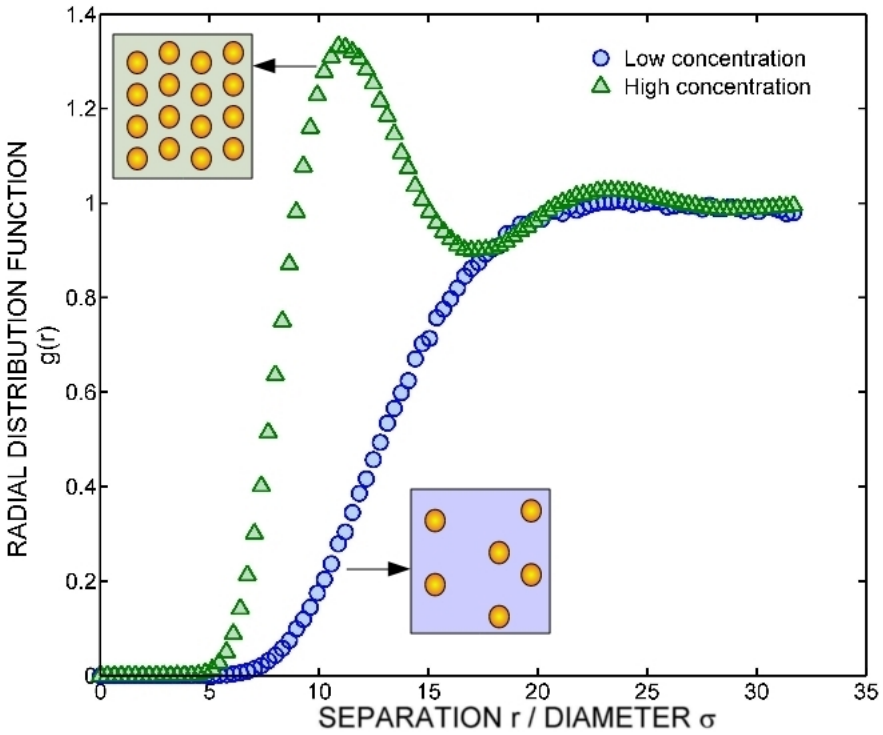

Figure 9: Radial distribution function for systems with varying particle concentration

As observed, the g(r) converges to unity for large separations. The qualitative reason for this convergance is that the g(r) can be seen as the correlation between a reference particle and other particles. Consequently, a particle that is a significantly large distance from another ceases to interact, no matter how strong the interactions at low separations, and so a g(r) with no interactions at those large separations converges to one.

Note that systems with different particle concentrations exhibit distinct differences. In relatively low concentrations, the g(r) gradually ascends to unity and then remains at that level. For larger concentrations, oscillation around $g(r) = 1$ are observed. The peaks in the curve represent particles that are located within a preferred distance from a reference particle. This is indicative of a crystal-like structure and can be seen particularly in cases were many-body contributions become important

due to an increased concentration. That is, the location of a particle is an influence of all the surrounding particle's additive effects when they are forced to be near many others. This particular trait will become important in the process that translates radial distribution functions into pair potentials.

3.4 Pair-potential of particle ensembles

The pair-potential, u(r), of an ensemble describes the interaction between a "pair" of particles in a certain medium. In order to translate the g(r) into a u(r), certain mathematical approximations are made in order to account the fact that the ensembles have a finite concentration and the interaction is not pair-wise in nature. In the limit of infinite dilution, with only two particles feeling each other, the u(r) is related to the g(r) through:

$$\lim_{n \to 0} u(r) = -k_B T ln[g(r)] \tag{15}$$

where k_B is the Boltzmann constant, $1.38 \cdot 10^{-23} \frac{J}{K}$, and T is the temperature of the system. For finite particle concentrations, the readily obtainable, experimental quantity from the radial distribution function is the so called potential of mean force, w(r) and defined as:

$$w(r) = -k_B T ln[g(r)] \tag{16}$$

Recall that in the previous section the radial distribution function has a strong dependence on particle density. Consequently the potential of mean force is sensitive to particle concentration through Eq. 16. While no exact relations exist between the pair potential and the potential of mean force, accurate approximations exist to perform such a transformation.

In this study, the Ornstein-Zernicke integral equation with appropriate closure

relations is used [27, 28]. The overall idea of the Ornstein-Zernicke equation is to separate the total correlation function, $h(r_{12})$, of a pair of particles separated a distance r_{12}, into a combination of a direct correlation function, DCF or $c(r)$, which is the direct effect between a pair of particles, and an indirect correlation function, ICF. In general form, the Ornstein-Zernike is written as:

$$h(r_{12}) = c(r_{12}) + n \int c(r_{13})h(r_{23})dr_3 \tag{17}$$

where the ICF is described as the convolution integral in the right hand side term that integrates all indirect correlations between particles 1 and 2 through all third particles that have a correlation with the pair of particles in interest. The total correlation function, $h(r_{12})$, is directly related to the radial distribution function through: $h(r_{12}) = g(r_{12}) - 1$. The Ornstein-Zernike equation introduces an equation that relates the radial distribution function to a new unknown function, the direct correlation function.

Consequently, Ornstein-Zernike equations are used in conjunction with closure relations that relate this direct correlation function to the pair potential [29].

One applicable closure relation, known for its accuracy for "soft" potentials, is the Hypernetted Chain (HNC) approximation. In general form, for any coordinate system, the HNC equation is [29]:

$$c(r_{12}) = g(r_{12}) - 1 - ln(g(r_{12})) - u(r_{12})/k_BT \tag{18}$$

The Ornstein-Zernike, together with the HNC closure relation, can be evaluated in two dimensions through [30, 31]:

$$u(r) = w(r) + n \cdot k_BTI(r) \tag{19}$$

where n is the number density of particles in each frame and I(r) is the convolution integral which is solved in an iterative fashion until convergence is achieved through:

$$I(r) = \int [g(r') - 1 - nI(r')] \, [(g|r' - r| - 1] \, d^2r' \tag{20}$$

After computing these quantities, the potential u(r) is readily available. Its worth noting that this procedure has some limitations. It has been observed that after relatively large concentrations, the convolution integral does not converge using Eq. 20 described above. Yet, for the systems sampled in this study, Eq. 19 provides accurate, convergant results.

The reliability of the HNC approximation is tested further in this study after Monte-Carlo simulations are introduced. The simulations are used to generate distributions with desired characteristics and the robustness of the HNC approximation in this form is tested.

3.5 Materials and methods to prepare dispersions in nonpolar solutions of nonionizable surfactants

Particle interactions are measured in nonpolar oils with non-ionic, non-dissociable surfactants. In order to perform this task, a glass cell is made in order to hold the dispersion and to be able to observe particles in a microscope in a 2-D plane. The glass cell is made by assembling a glass ring onto a coverslip and sealing them with optical adhesive (Borland NOA-81), cured under a UV lamp. Inside the cell, a cover slip wedge is made out of polymer-coated cover slips; a schematic of the setup is shown in Figure 10.

The glass cell's base is a large microscope cover slip. The glass ring will contain the solution when performing an experiment and seen under a microscope. The glass wedge is used as a mechanism to confine particles in a quasi-2-dimensional setup. The advantages of the wedge geometry is two-fold. The necessity for a 2-dimensional setup means that the wedge must confine vertical Brownian motion, while not affecting

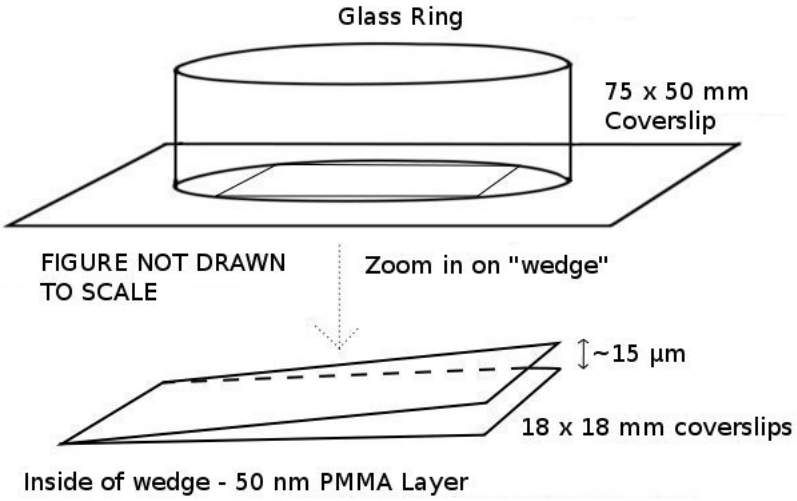

Figure 10: Microscope cell made out of thin, microscope quality glass

motion in the horizontal direction. Consequently, particles are forced to remain at the same height, a requirement for video microscopy experiments. If, for example, a top slip would not be used and a dispersion is placed under the microscope, the results are images of particles coming in and out of focus, an undesirable trait. Second, a wedge geometry, while providing a relatively flat sandwich-type enclosure with a negligible height difference for the field of view of the microscope, allows access to different plate separations between the glass plates to be readily accessible by moving the microscope stage. Without prior knowledge of the interaction between particles, the ability to tailor the separation between confining plates is crucial to make accurate measurements.

The purpose of polymer films coated onto the inside of the viewing wedge is to prevent particle attachment to the flat surfaces by providing a repulsive force of the same nature as inter-particle repulsions. The small coverslips that make the wedge are coated with a thin layer of Poly-methyl methacrylate, PMMA. In order to perform this task, a solution of 30 g/L is made by dissolving PMMA pellets in Toluene. Coverslips are placed on a spin-coater and covered with the PMMA solution using a simple dropper. The spin-coater is then started at a rotating speed of 1000 rpm for a

duration of one minute. These settings make a thin, even, film of approximately 75 nm of polymer on the glass substrate [32].

The solvent used in this study is Hexane (Sigma Aldrich, ACS grade) and the non-ionic surfactants used are Sorbitan trioleate, tradename Span 85 and Sorbitan monooleate, tradename Span 80. The particles used in this section are PMMA microspheres, $1.08\mu m$ in diameter from Bangs Laboratories disperse in an aqueous solution by the manufacturer. In order to prepare particle dispersions in nonpolar media from particles in original aqueous solutions, a method called solvent swapping is used to transfer particles between fluids, water and Hexane, and obtaining relatively pure dispersions. The idea of solvent swapping is to transfer polymer particles between two immiscible fluids through the transfer onto an intermediate solvent with partial miscibility in both fluids.

Particles in the original aqueous solution are sonicated and the desired volume for further analyses is extracted. The extracted dispersion is then diluted in pure water, sonicated, centrifuged, and the supernatant fluid removed. This dilution process is repeated at least three times in order to clean the particles and remove any impurity that comes dissolved in the water dispersion (e.g. aqueous dispersion stabilizers). In the next step particles, with as much water removed after the supernatant extraction process, are diluted in isopropanol, a fluid miscible in both water and Hexane. The particles are cleansed again through repeated sonication and centrifugation. Finally, the intended fluid, Hexane, is used as dilutant for the dispersion and the process is repeated again in Hexane in order to clean the particles and remove as much of the intermediate fluid, isopropanol, as possible. A graphical depiction of the solvent swapping process is shown in Figure 11.

In solvent swapping, the larger the number of sonication and centrifugation cycles with each solvent at a time, the lower the concentration of impurities as the solvent extracts impurities with each cycle. including trace amounts of the previous solvent.

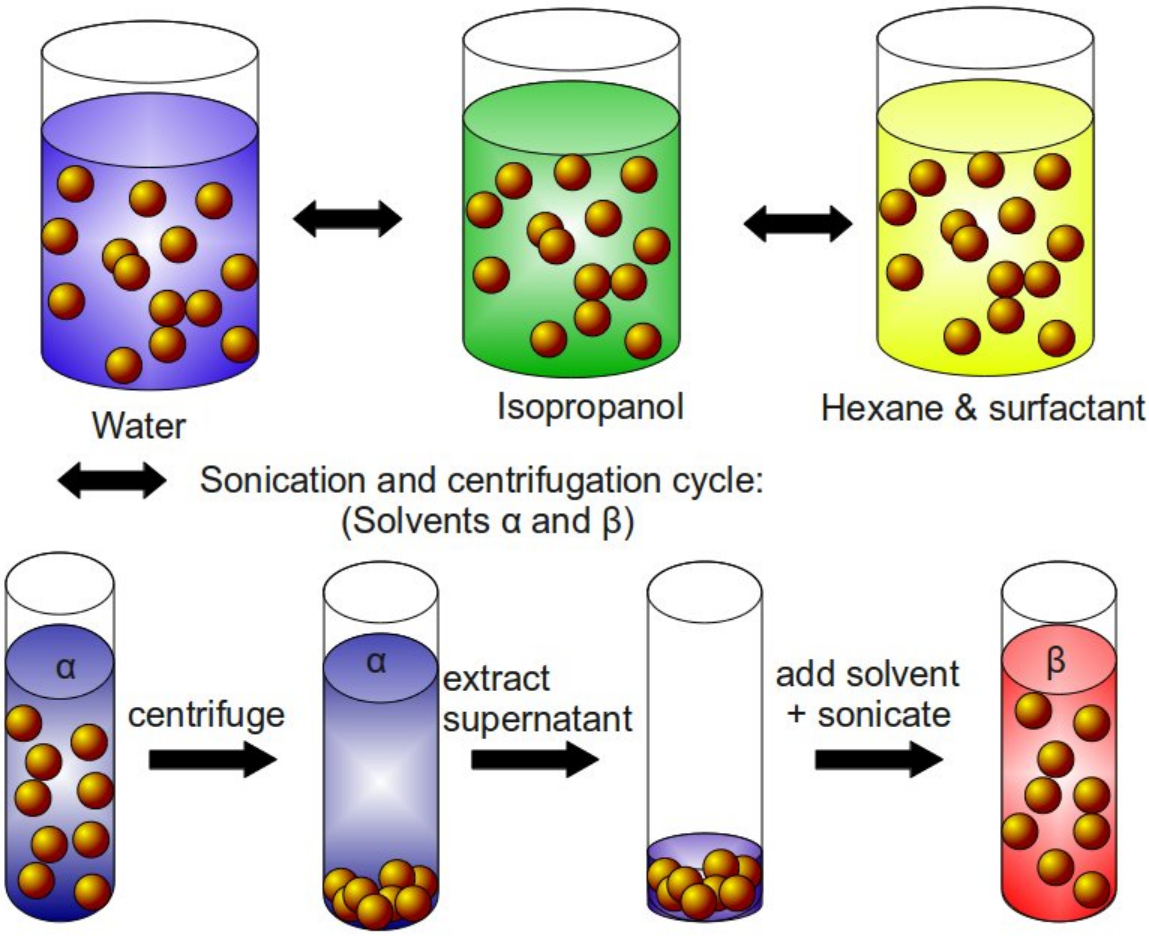

Figure 11: Graphical depiction of the solvent swapping process involving repeated sonication and centrifugation of polymer particles in carefully chosen solvents. (Top) Particles are transferred from an aqueous phase to a Hexane phase through an intermediate isopropanol phase. (Bottom) One cycle of the sonication + centrifugation process

In this study, three cycles of sonication/centrifugation were used with each solvent. The measure used to show that the number of cycles performed are enough is the final water content of the Hexane-based dispersion. Studies using Karl Fischer titration have shown that the water content of pure Hexane is below 0.003 wt%. The dispersion in Hexane prepared after the solvent swapping process contains similar amounts of water that was originally in the pure Hexane solution [16]. This is evidence that indeed the solvent swapping process is adequate at transferring particles from an aqueous phase into an oil phase without significant water contamination.

The materials used in this section were carefully selected with the following thoughts in mind. Hexane was chosen as the solvent because it is one of the least polar solvents there are, with a dielectric constant of $\varepsilon = 1.89$. Despite its low polarity, solutions of Hexane with nonionizable surfactants show promising preliminary results of substantial conductivity increases for a rising surfactant concentrations [15]. Furthermore, the optical contrast between Hexane and the particles is large; a quantitative measure of optical contrast is the refractive index difference between the solvent and the solid material. The refractive index of Hexane is 1.375 while the refractive index of PMMA is 1.49 [33]. In particular, light scattering experiments required such optical contrast, with which successful characterization of the size and shape of the aggregate micellar structures where characterized with; important background for this work [16].

CHAPTER IV

PARTICLE DISPERSIONS IN NONPOLAR OILS

4.1 Results & Discussion

4.1.1 Effect of Oleate-based surfactant Span 85

Particle interactions were determined for PMMA particles dispersed in Hexane with varying concentrations of Span 85. The size of the particles for this experiment is 1.08 μm in diameter. Span 85 concentrations ranging from 0.5 mM to 50 mM in Hexane were sampled.

A microscope image of a typical ensemble of PMMA particles in Hexane is shown in Figure 12.

A video microscopy experiment consists of a compilation of many images like Figure 12. A typical experiment would consist of 60,000 continuously captured images, which at a typical acquisition rate of one image per second, would last about 18 hours to complete. The reason for the extended duration of the experiment is that a sufficient amount of images is required in order to have good statistical accuracy on the radial distribution function, g(r), calculated from such images. A review of the statistical accuracy of the experiments and their g(r) is made on the Monte-Carlo simulation section of this study.

Radial distribution functions were obtained for dispersions with varying Span 85 concentration and are shown in Figure 13:

In Figure 13, the curves show that the range of interaction decreases with increasing surfactant concentration. That is, particles are able to approximate each other

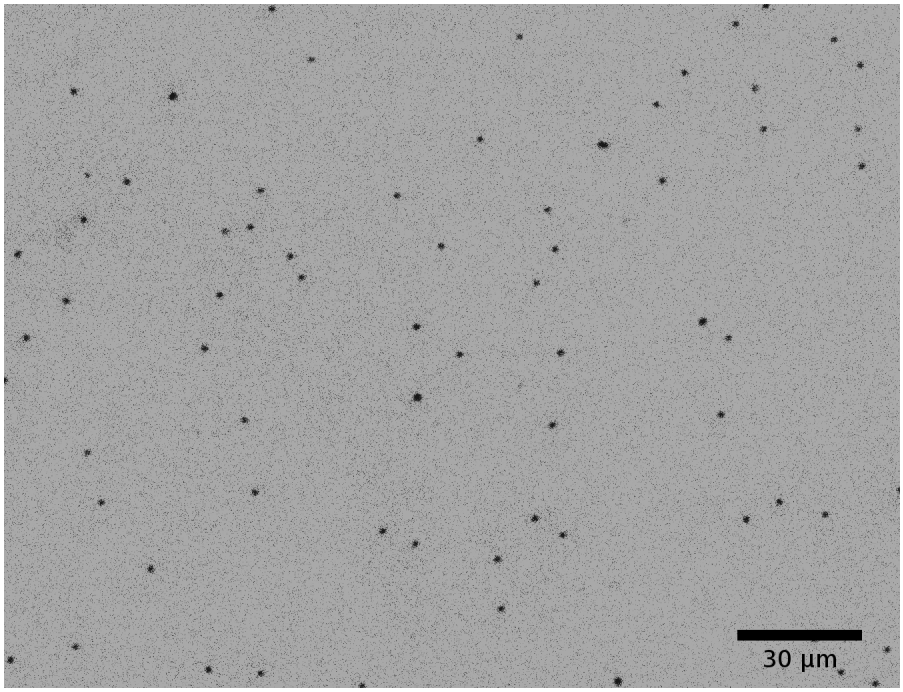

Figure 12: Colloidal dispersion of PMMA particles in Hexane with 10.0 mM Span 85

more so at higher concentrations. The g(r) additionally show that the interactions in this study are soft in nature. That is, there is a gradual increase in the g(r), in contrast say to a sharp or vertical increase in g(r) as would be the case of non-interacting hard spheres [34]. This is the first piece of evidence that there is an electrostatic interaction between particles. The g(r)'s are then further processed, as mentioned in the methods section, to a pair-potential utilizing the HNC approximation. The resulting potential can be seen in Figure 14:

4.1.2 Discussion - Interaction in the framework of a Screened-Coulomb potential

Before starting with the discussions on the results, the nature of the surfactant Sorbitan trioleate, Span 85 will be briefly discussed. Span 85 can be seen as a three-legged oleate as seen in Figure 15.

The molecular structure of Span 85 is based on a cyclic 5-membered ring with three long hydrocarbon tails. The cyclic ring is the hydrophilic portion of the surfactant.

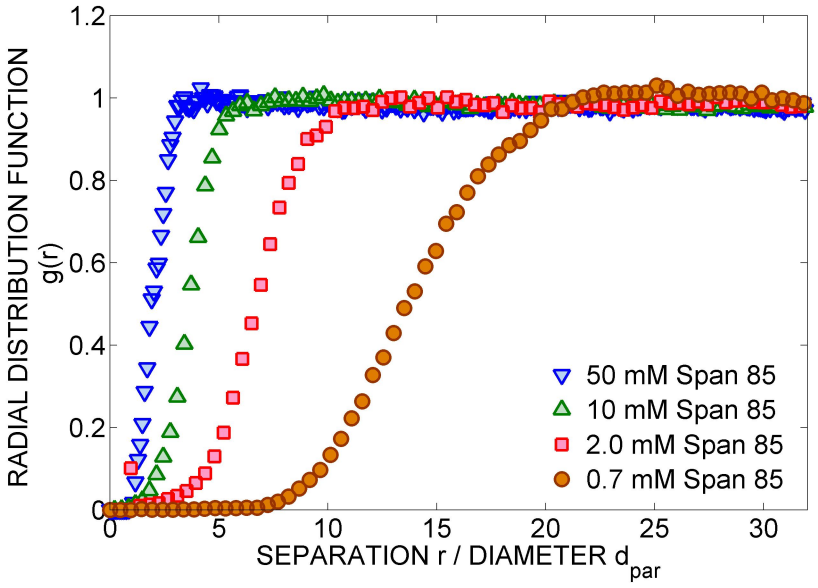

Figure 13: Radial distribution function of PMMA particles ($1.08\mu m$) in Hexane at changing concentrations of Span 85

In Figure 15, it is readily apparent that there is no dissociable group available in the molecule itself; an important distinction as electrostatic effects involve dissociation of ions. Yet, the results show that increasing concentrations of Span 85 in Hexane work to stabilize a polymer dispersion against aggregation with a strong interaction potential between particles.

In order to determine what form the potential takes, the potential was fitted to a variety of possibilities, the most relevant being the screened-Coulomb potential as the objective is to determine whether or not the interactions are electrostatic in nature. Recall the screened Coulomb potential between particles of diameter, d_{par}:

$$u(r) = \frac{(Z^* e)^2}{(4\pi\varepsilon\varepsilon_0)\, r} \frac{exp(\kappa d_{par})}{\left(1 + \frac{\kappa d_{par}}{2}\right)^2} exp(-\kappa r) \tag{21}$$

In Eq. 21, the surface charge is measured in terms of the effective charge number. The effective charge number is directly related to the ζ-potential through:

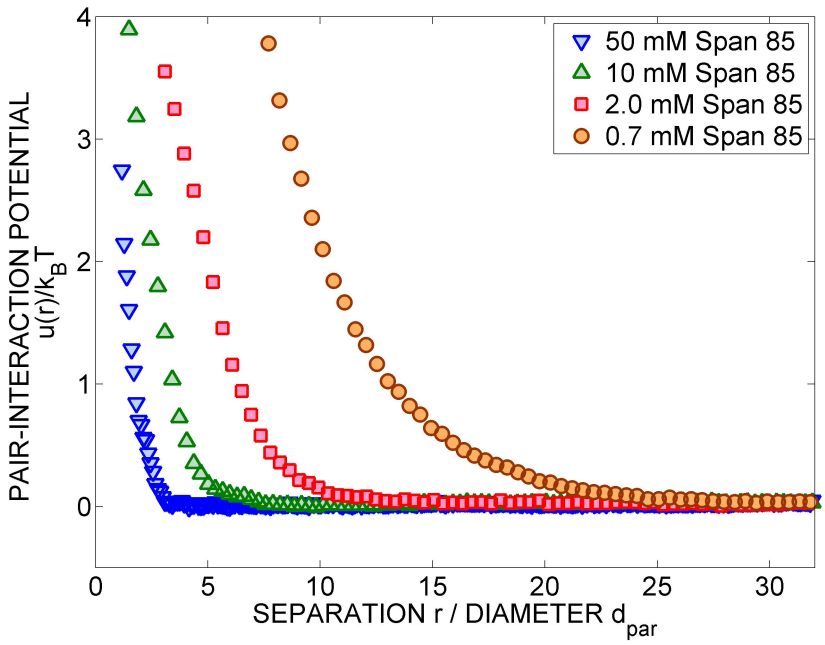

Figure 14: Pair-interaction potential of a PMMA particle dispersion in Hexane at different Span 85 concentrations

$$Z^* = \frac{d_{par}(1+\frac{\kappa d_{par}}{2})}{2\lambda_B}\frac{e\zeta}{k_B T} \tag{22}$$

The advantage of looking at relationship for a ζ-potential is because in colloid science it is a measure of a dispersion's stability against aggregation, more so than is the effective surface charge. Consequently, an equivalent form of the screened-coulomb interaction in terms of a ζ-potential is:

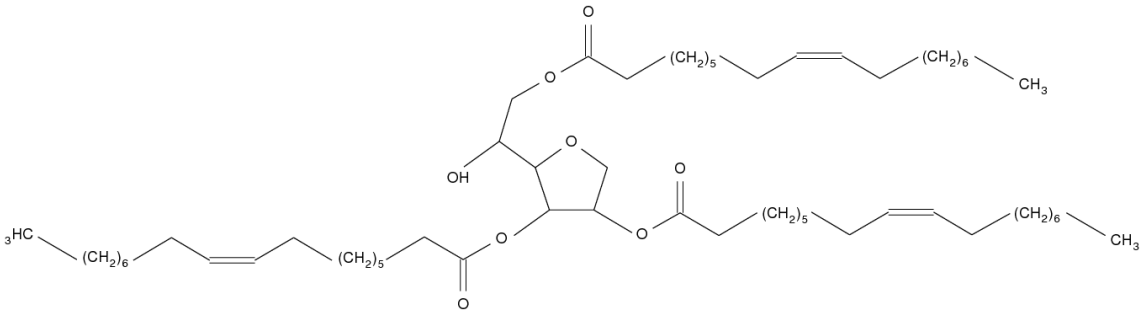

Figure 15: Chemical structure of Sorbitan trioleate, tradename Span 85

$$\frac{u(r)}{k_B T} = \left(\frac{e\zeta}{k_B T}\right)^2 \frac{d_{par}^2}{4\lambda_B} \frac{e^{-\kappa(r-d_{par})}}{r} \tag{23}$$

In order to determine the appropriateness of the fit, Eq. 21 can be rearranged into:

$$ln[r \cdot u(r)] = ln\left[\frac{(Z^* e)^2}{(4\pi\varepsilon\varepsilon_0)} \frac{exp(\kappa d_{par})}{\left(1+\frac{\kappa d_{par}}{2}\right)^2}\right] - \kappa r \tag{24}$$

Consequently, a plot of ln(r*u(r)) vs. r is used determine whether a straight line fit is adequate for the data and is shown in Figure 16:

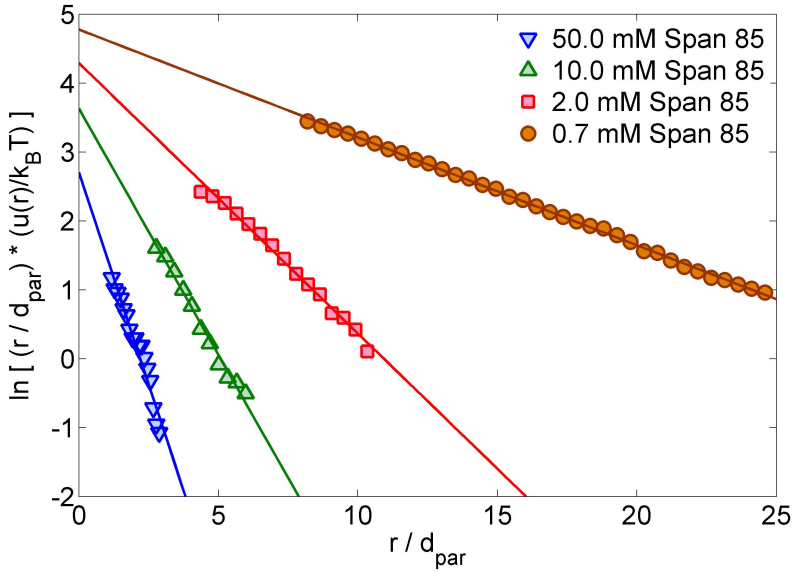

Figure 16: Rearranged plot of ln[r u(r)] vs. r PMMA particle dispersion in Hexane at different Span 85 concentrations

A linear fit is applied to the curves in Figure 16; and appropriate fits are observed. First, the fact that a screened Coulomb equation fits well is a strong indication that the interaction is indeed of such a form. Fits to other possible potentials, different to the screened-Coulomb, are mentioned in further sections and shown how they don't agree with experimental results.

Several key pieces of information can be obtained from the linear fits. First, note

in Eq. 24 that the slope of the curves in Figure 16 is the inverse Debye length, κ. The Debye length is a measure of the amount of ions in solution, and therefore the conductivity, as the smaller the Debye length, the larger the amount of ions that "screen" the charges. Furthermore, the effective charge number can be extracted from the plot's intercept. Note that in Eq. 24 all other variables are known except for the effective charge number. The effective charge is the magnitude of adsorbed charges to the particle surface.

It's necessary to mention that only a portion of the interaction potential curves in Figure 14 are used for the ln (r u(r)) vs. r plots. The underlying reason for using only a selected portion of the data is based on statistical reasons and the natural behavior of Eq. 24. On the left-hand side of Eq. 24, as a potential approaches zero, a natural phenomena for interactions at large distances, the more the logarithm term exponentiates natural experimental scatter in the data, $\lim_{x\to 0} ln(x) = -\infty$. To prevent analyzing error enhanced sections of the potential, as $u(r) \to 0$, a reasonable empirical choice is made to make $0.1k_BT$ a lower bound for the interaction energy used in Figure 16.

Second, statistical precision of experimental data at low separations, which translates onto higher potentials, is relatively low. Statistical mechanic theory states that the probability of finding two particles at a separation r that experience a potential u(r) between them is exponentially decreasing with respect to separation given by the Boltzmann factor: $exp(-u(r)/k_BT)$. High interaction energies between repulsive particles, at low separations, are seen in rare occasions and so the u(r) vs. r data has a natural scatter at high interaction energies. Again an empirically- determined cut off is made to make an upper bound interaction energy of 4 k_BT to be utilized for further analysis, the fits to the screened-Coulomb.

Notice the magnitudes of the ζ-potentials in Table 1. The ζ-potentials are in the same order of magnitude as those of dispersions in aqueous systems, which for latex

Table 1: Table of parameters of the fit to the data in Figure 16 with Eq. 24

[Span 85] (mM)	Particle concentration ($10^{-3} n d_{par}^2$)	κ^{-1} (μm)	Z*	ζ-Potential (mV)
0.7	1.09 ± 0.15	7.06	62.83	82.3
2.0	1.36 ± 0.33	2.82	48.75	57.7
10	1.85 ± 0.25	1.51	34.90	36.3
50	2.03 ± 0.24	0.82	21.41	18.2

particles in water at several pH range between 10 - 100 mV [35]. This information is very unexpected as the results show that non-ionic and non-dissociable surfactants in nonpolar fluids introduce similar magnitudes of potentials as charged aqueous systems.

The effective charge numbers, on the other hand, differ significantly in magnitude to those in aqueous systems. The concentration of charges on particle surfaces in nonpolar oils in this study is vastly smaller than the concentration of charges on comparable surfaces in aqueous systems. The range of the values of Z* in this study are between 10 and 100 charges, see Table 1. In aqueous systems the Z* values are in the order of 10^3 to 10^5 charges [36]. The reason for the contrast in having comparable magnitudes of ζ-potentials yet large differences in magnitude in effective charge numbers is that the solvent's polarity comes into play when calculating ζ-potentials.

As seen in Eq. 22, the effective charge number is proportional to the ζ-potential but inversely proportional to the Bjerrum length, λ_B. The Bjerrum length at room temperature is 0.7 nm for aqueous systems yet is 28 nm for nonpolar oils ($\varepsilon = 2$). The contribution to the potential of a charge in a nonpolar oil is much larger than the contribution of a charge in an aqueous system. The few charges adsorbed to the surface of the particles in the dispersion in nonpolar oils with non-ionic surfactants are apparently enough to stabilize the colloidal dispersions.

The screening lengths, κ^{-1}, sampled in this study are in a much larger range

than what can be seen in aqueous systems. The κ^{-1} measured in this study for the nonpolar oil Hexane is in the order of 1 to $10\mu m$. Notice that at the lowest stable data point shown in Table 1 at 0.7 mM Span 85 in Hexane, the screening length is 7.08 μm. In comparable aqueous dispersions, κ^{-1} are in the order of $100nm$ or less for larger ionic strengths [36]. This means that Debye screening lengths are at least an order of magnitude larger considering the results in this study. Considering that polar fluids such as water are compared to nonpolar fluids, such as Hexane, this is not entirely unexpected. Large screening lengths refer to low ionic strengths in the fluid, and hence lower conductivity as well.

There are other interaction potentials that were considered as suitable candidates for particles in nonpolar oils. Some reports of polymer particle dispersions in nonpolar oils with ionic surfactants have shown that a counter-ion only model reflects the pair-interactions reflected by a power law, rather than by a screened-Coulomb, Eq. 21. In 2002, Briscoe and Horn utilized a surface force apparatus to measure the interactions between mica spheres disperse in Decane containing millimolar concentrations of AOT above the CMC. Their main conclusion is that the potential fits to a counter-ion only model where the potential scales with the inverse of the separation $\frac{1}{r}$ [12]. Different to the results in this study were screening is evidenced above and below the CMC of the Span-based nonionizable surfactant, the model by Briscoe shows that no observable screening effects are observed below the CMC of ionic surfactants in nonpolar liquids.

A double-logarithmic plot of the interaction potential clearly shows that the experimental data are <u>not</u> consistent with the power-law behavior predicted by counter-ion only theory, see Figure 17. In contrast to a fit to a screened-Coulomb type of interaction, Figure 16, the pair-potential plotted assuming a power law dependance has a distinct curvature, illustrated by the presence of a linear asymptote, Figure 17.

In 2005, Hsu et al. reported a screened-Coulomb potential for dispersions in nonpolar media with ionic surfactants as charge control agents, substances which

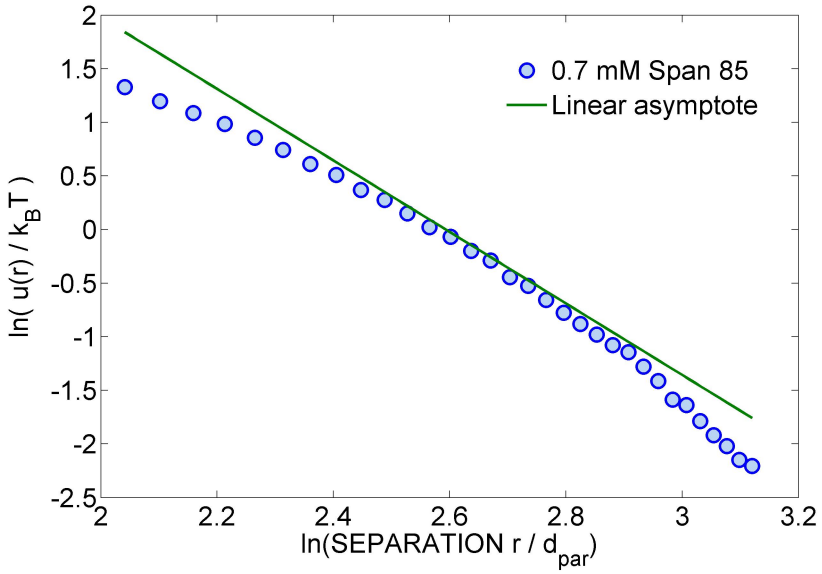

Figure 17: Double-logarithmic plot of the ln(u(r)) vs. ln(r) for a particle dispersion in 0.7 mM Span 85 in Hexane (markers) with asymptote (line)

in varying concentrations control the amount of ions in solution and the amount of surface charges, exclusively in micellar regimes [1]. Sainis et Al. reports an unscreened interaction below and screened interaction above the CMC for AOT in nonpolar liquids. This report proves that screened interactions takes place below and above the CMC, where the difference is the use of the nonionizable surfactant rather than an ionic one. Therefore a screened-Coulomb potential is not a trivial expectation for particles in a nonpolar oil. The implications of a screened-Coulomb potential are that surfaces charge and bulk nonpolar solutions charge both above and below the CMC.

4.1.3 Effect of Oleate-based surfactant Span 80

In the previous section, the charge control capabilities of Span 85 in Hexane were analyzed. Now, the same analysis will be performed except that a different surfactant, Sorbitan monooleate known as Span 80, will be used. The molecular structure of Span 80 is shown in Figure 18

Comparing Span 80 with Span 85, (Figures 15 and 18) it can be readily seen that

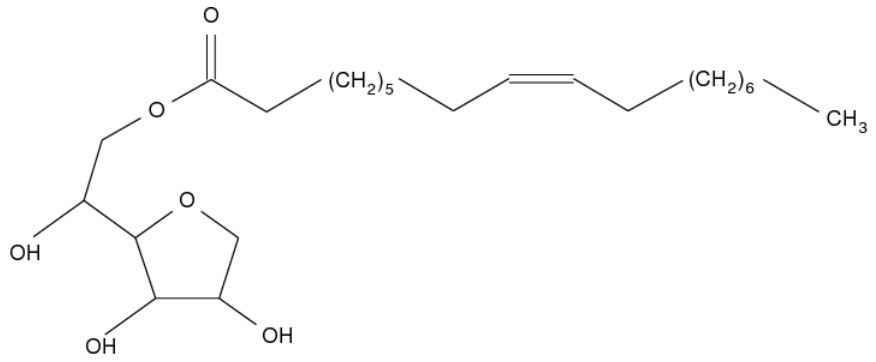

Figure 18: Molecular structure of Sorbitan Oleate, also known as Span 80

the molecules are very similar with the same functional groups. The main difference between the two molecules is that Span 80 contains only one strand of hydrophobic hydrocarbon chain while Span 85 contains three. In Span 80, instead of the missing two hydrocarbon chains there are only hydroxyl groups. The important difference between the surfactants is that span 85 forms small, spherical micelles while Span 80 forms large, worm-like micelles, evidenced by light scattering experiments [16].

Polymer dispersions using the same particles and fluid as in the previous experiment, PMMA particles ($1.08\mu m$) in Hexane, are made with varying concentrations of Span 80. The concentrations range from below the CMC to above the CMC of Span 80 at concentrations of 0.5 mM, 0.75 mM and 2.0 mM. The radial distribution functions of such experiments are shown in Figure 19.

Due to the formation of relatively small amount of dimers in solution, at separations of 1 to $3d_{par}$, the g(r) shows small dimer peaks. These peaks are expected as no matter how much experimental care is taken in making clean dispersions, there is always a small amount of dimer formation.

The g(r)'s were then transformed into u(r)'s through the HNC approximation; the resulting potentials are shown in Figure 20.

The interaction potentials are then fitted to the screened-Coulomb potential by plotting the data in $ln(r \cdot u(r))$ vs. r form with the following results:

The parameters obtained from the fit to the curves in Figure 21 are shown in

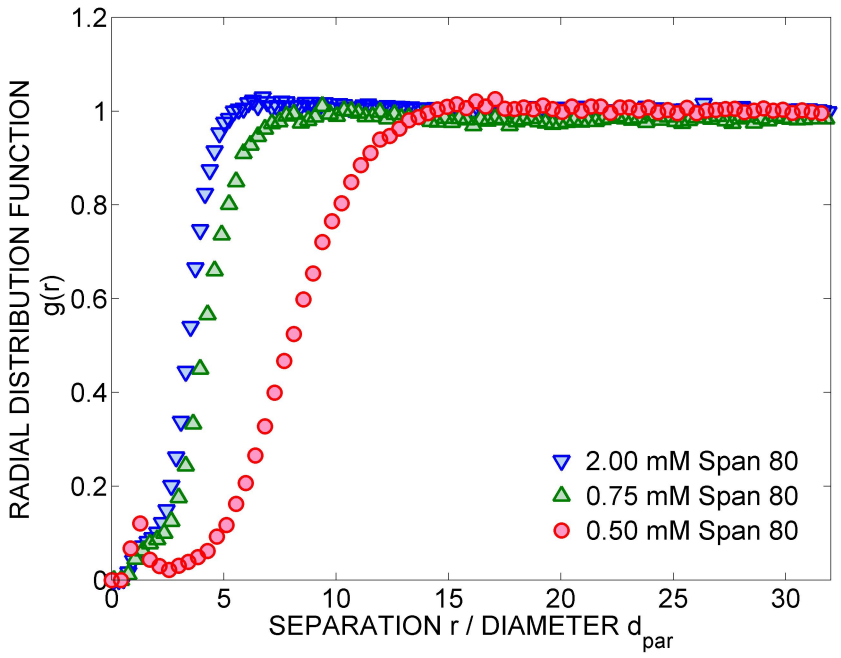

Figure 19: Radial distribution function, g(r), of a PMMA particle dispersion in Hexane with varying concentrations of the surfactant Span80

Table 2.

Table 2: Table of parameters of the fit to the data in Figure 21 with Eq. 24

[Span 80] (mM)	Particle concentration ($10^{-3} n d_{par}^2$)	κ^{-1} (μm)	Z*	ζ-Potential (mV)
0.50	2.02 ± 0.44	3.48	45.87	57.0
0.75	2.32 ± 0.48	1.39	45.75	47.0
2.00	3.00 ± 0.37	0.76	106.14	85.7

Comparison between Span 80 and Span 85

In general, κ^2 is proportional to the number of ions in solution, which should scale like $exp(-\lambda_B/d)$ where d is the ion diameter. Larger micelles means Debye lengths should be smaller; exactly what is observed in Table 2. The effective surface charges, $Z*$, are in the same order of magnitude.

The amounts of required surfactant needed to decrease the screening length, reflective of an increase in ion conductivity in solution, is less for Span 80 as compared

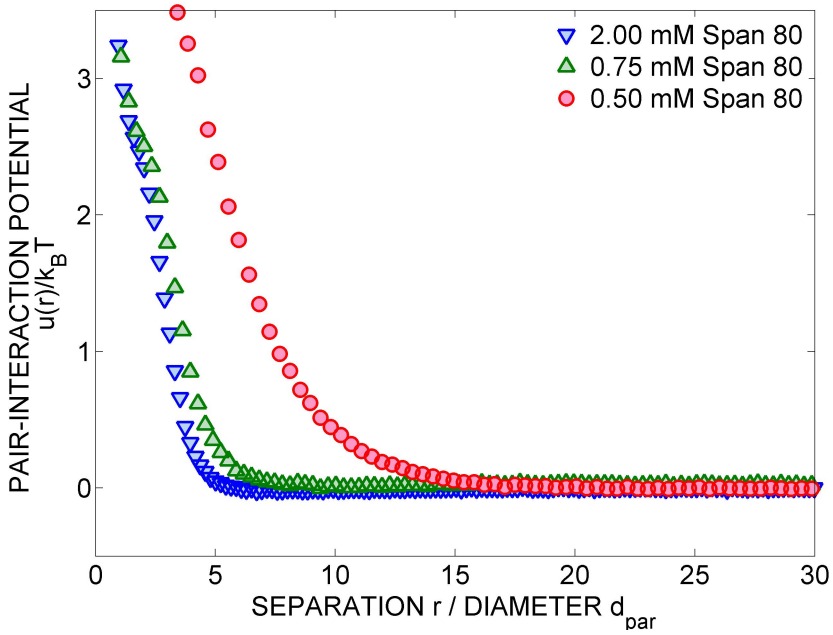

Figure 20: Pair-interaction potential of a PMMA particle dispersion in Hexane with varying concentrations of the surfactant Span80

to Span 85 reflected by the lower CMC, and the larger aggregate structures with Span 80. By looking at Tables 1 and 2, it can be seen that at a concentration of 2.0 mM Span 80 in Hexane, the screening length is $\kappa^{-1} = 0.76\mu m$, compared to $\kappa^{-1} = 2.82\mu m$ for Span 85.

4.1.4 Particle interactions in Decane

The solvent used extensively in this study is Hexane ($\varepsilon = 1.89$); there are many other nonpolar solvents to test. In particular, a test was made in order to quantify the relative effect nonionizable surfactants have on a longer hydrocarbon liquid such as Decane ($\varepsilon = 2.01$). A particle interaction experiment was made using 2.0 mM Span 85 in Decane which can be readily compared to that result for Hexane. The g(r) of such an experiment is shown in Figure 22.

In Figure 22, the g(r) and the u(r) match relatively well. The results show graphically that different hydrocarbon solvents, Hexane and Decane, respond equally to the

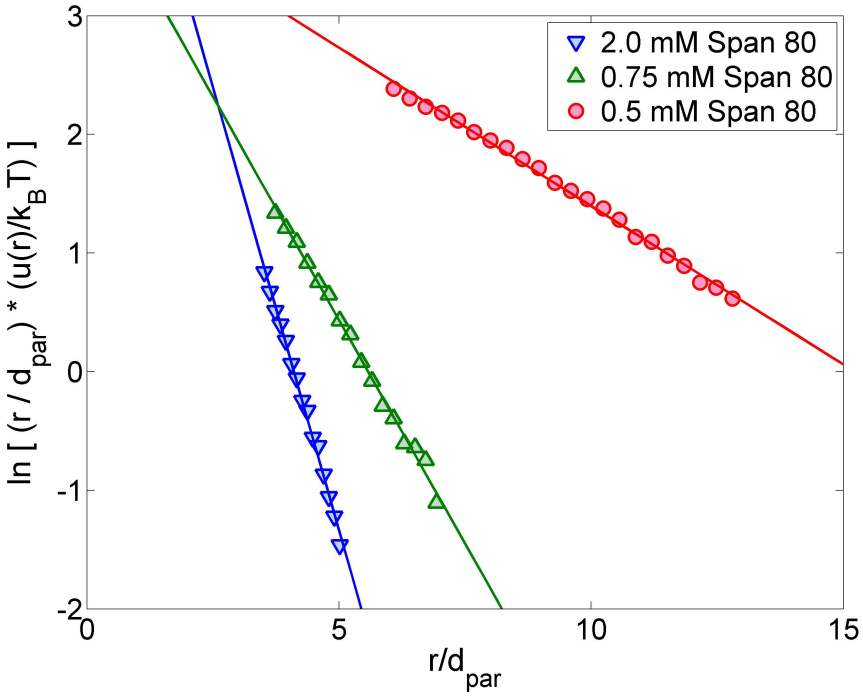

Figure 21: Plot of $ln(r \cdot u(r))$ vs. r with best fits to the screened Coulomb potential

nonionizable surfactant Span 85. In order to detect the effect of the small differences in solvent polarity ($\varepsilon = 1.89$ for Hexane and $\varepsilon = 2.01$ for Decane, the potentials are fit to a screened-Coulomb from where κ^{-1} and Z^* are extracted for each solvent, Table 3.

Table 3: Table of parameters, κ^{-1} and Z^*, from screened-Coulomb fits to the pair-potential of particles in Hexane and Decane

Solvent	κ^{-1} (μm)	Z^*	ζ-potential (mV)
Hexane	2.79	51	59.8
Decane	3.44	47	54.4

As can be seen, the effective surface charge numbers are close to each other, yet, there is a 23% increase in the Debye length in Decane as compared to Hexane. The differences in dielectric constant, from 1.89 to 2.01, are reflected it seems in the Debye length.

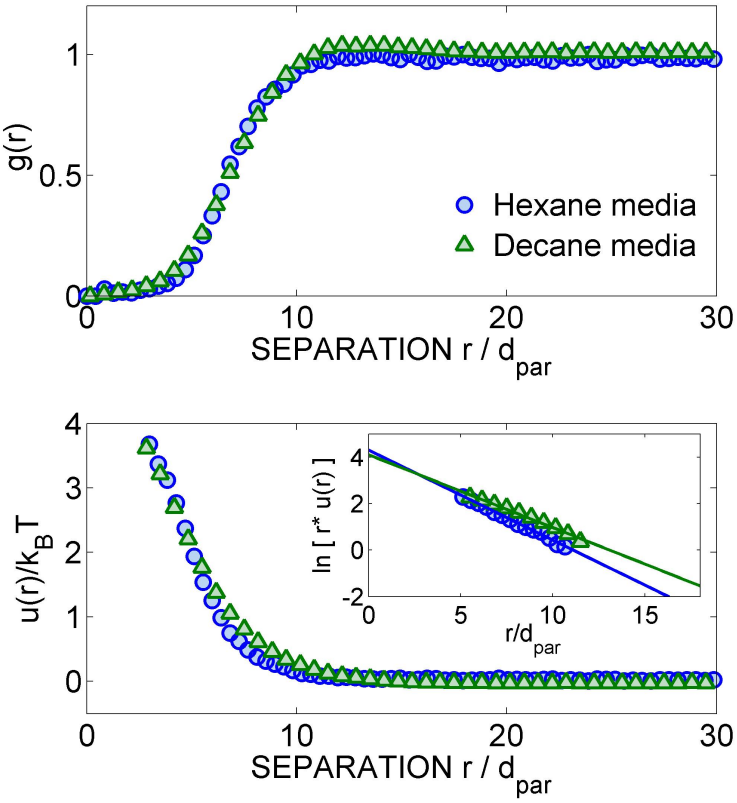

Figure 22: Radial distribution functions(top) and pair-interaction potentials (bottom) for PMMA particles ($1.08\mu m$) in 2.0 mM Span 85 in Decane and 2.0 mM Span 85 in Hexane. The inset is the linear fit of the potentials to the screened-Coulomb equation

4.1.5 Effect of inter-plate height

Particle interactions measurements have been taken assuming that there is no effect due to the plates confining the particles in two dimensions. In order to assess the validity of this assumptions, an experiment was made to look at the interaction measurements at different inter-plate heights. If an effect due to the presence of the wall's is significant, then changing the inter-plate height would show whether or not there is indeed an effect due to the walls.

Experiments are made using a PMMA particle dispersion ($1.08\mu m$) in Hexane. Separate experiments consist of looking at the dispersion locally at different positions

in the wedge consisting of different inter-plate heights. The microscope has a height detector that displays the distance, z_{focus}, between the objective and the image in focus; the inter-plate height is readily available by taking the difference between the height of the upper surfaces of both coverslips forming the wedge. These surfaces are "visible" thanks to small impurities, scratches or deposited particles. The error in these separation measurements arising from the finite focal depth of the microscope objective is 1 μm given by the manufacturer.

Two experiments are made at two different inter-plate separations, 8.25μm and 20.15μm. The g(r) and the u(r) for the experiments are shown in Figure 23.

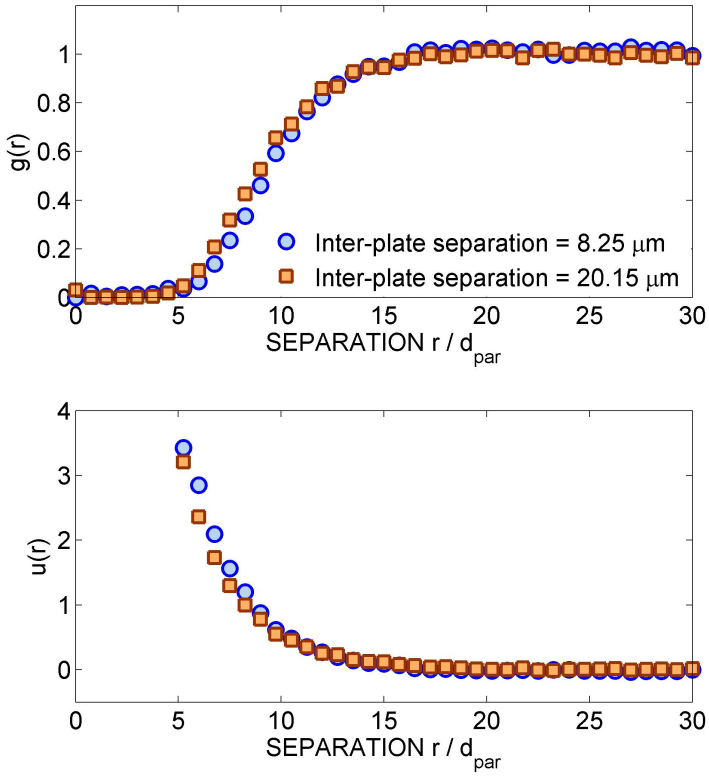

Figure 23: Radial distribution function, g(r), vs r for particle ensembles in 2 mM Span 85 in Hexane at different inter-plate heights (Top) and corresponding pair-interaction potentials, u(r) vs r (Bottom)

As can be seen, changing the inter-plate height does not change the interaction

between the particles substantially as observed by the interaction potentials. Therefore, it appears safe to assume that the width of the confining gap does not affect the lateral particle interaction, but only serves to suppress out-of-plane fluctuations of the particle positions.

4.1.6 Limitations to the method

The methods utilized in this study are not of the kind that would allow precise bookkeeping of the uncertainties in the data processing. This can be explained by looking at the different sections of the experimental procedure. Before beginning an experiment, one designs and estimates how many images are needed to get a reasonably smooth radial distribution function, g(r). For example in this study, at least 60,000 images were recorded for each experiment with each frame containing anywhere between 20 and 100 particles. Overall, this meant that one could obtain anywhere between $1.2 * 10^5$ to $6 * 10^6$ particle positions; far more than are used in typical video microscopy experiments to ensure adequate statistics [1]. Experimentally it was determined that the range in the number of particle positions aforementioned is enough to obtain a smooth g(r).

It is trivial that the more the number of images used in a certain experiment, the smoother the resulting g(r). Therefore there is no reproducibility in the design of the experiment in order to assess uncertainty; rather, there is only an increase in accuracy in the data the more the number of images used. It is precisely for that reason the number of data points obtained in this study is above what's currently performed in the field. Furthermore, observations when making these experiments show that for a relatively small amount of frames, the g(r) has relatively more deviations from a mean compared to experiments that have more frames. A graphical representation of such convergance is shown in Figure 24. Throughout this study, all video microscopy experiments are above the 60,000 frame threshold shown in Figure 24.

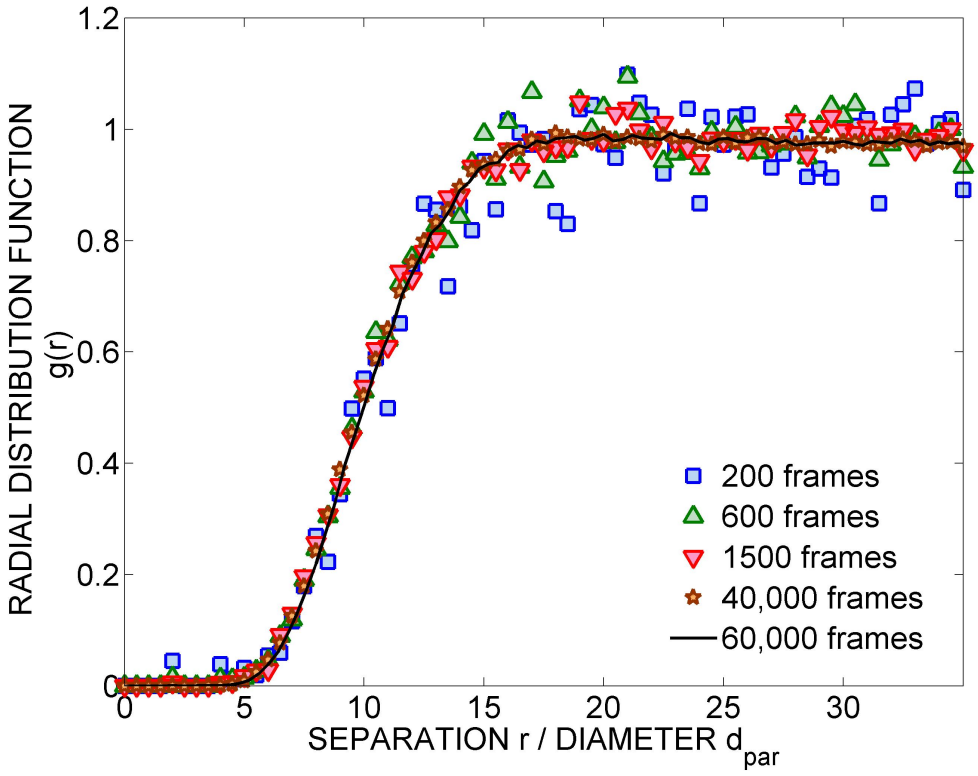

Figure 24: Sets of radial distribution functions calculated by considering a specific number of frames to show how the larger the number of states or frames used in an experiment, the smoother the g(r).

Another consideration to take into account is interaction potentials are the main measurements in this study. Yet, error propagates in a complicated fashion when converting a g(r) into a u(r). In particular, the convolution integral shown in equation 20 propagates error non-locally and iteratively. Non-local error propagation in the convolution integral occurs because the computation of the pair potential at a particular separation does not depend only on the value of the radial distribution function at that separation as seen by I(r), Eq 20. The computation of I(r) occurs by solving it recursively through many iterations until the function converges. As of now, there is no exact solution to many-body interactions; but, the Ornstein-Zernicke equation with the Hypernetted Chain Approximation has been tested in other systems and shown to work accurately [29]. Regardless, in the next section, simulations will be

used to test the reliability of the HNC procedure.

4.2 Monte-Carlo Simulations

Monte-Carlo simulations of colloidal interactions are the way this study uses to assess the validity of the resulting data obtained from the experiments. In addition, it is a method that can be used to test the validity of the procedures used in this study to obtain interaction potentials from the spatial arrangement of equilibrium ensembles. The importance of using such an experiment is that a particle distribution obtained from experiments, and characterized by the g(r), can be compared to a distribution generated from a simulation.

4.2.1 Monte-Carlo Background

Monte-Carlo Simulations are statistical computations with which one can approximate a physical system or solve mathematical problems with the use of random input with defined distributions. The methods were developed by scientists Ulam, Neumann and Metropolis in the 1940's in the Los Alamos Laboratory. The authors defined the Monte-Carlo Methods as, " a statistical approach to the study of differential equations, or more generally, of integro-differential equations that occur in various branches of the natural sciences" [37]. Monte-Carlo simulations give equilibrium information on system ensembles, in contrast to Browning Dynamics simulations commonly used to simulate kinetic phenomena between colloidal systems. The equilibrium arrangement of experimental ensembles is studied in this project; consequently a Monte-Carlo simulation is preferred in this study to model the spatial arrangement of particles.

The Monte-Carlo method relevant to this study is called the Metropolis Method [37]. The Metropolis method takes a system in one equilibrium state and translates it into another equilibrium state by allowing random particle motion that meets an energetic probability related to that move. Allen and Tildesley describe such a method

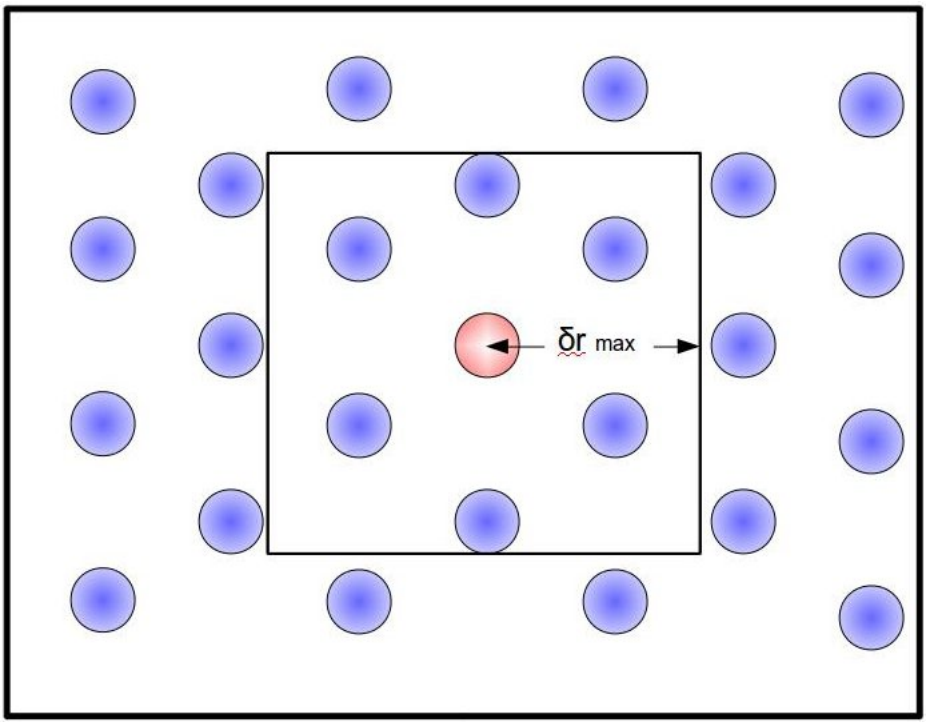

Figure 25: Representation of maximum allowed displacement a particle can travel in a loop of the Metropolis method

extensively [38] and an overview on procedures specific to this work are henceforth given. A Metropolis method falls under the category of being a Markov Chain type of algorithm; a sequence of memory-less, random events. The algorithm to perform such a move is as follows: A 2-D ensemble is created by specifying a certain number of particles inside a square of defined dimensions. The type of interaction between particles in the dispersion must also be specified in the form of a pair-potential, $u(r)$. A particle, i, in the ensemble is selected and given a random displacement, that can be no greater than a specified maximum displacement, δr_{max}. A representation of the allowed space a particle can move to is shown in Figure 25.

Once a move is made, a certain method must be used to determine if the move was favorable or in equal relative probability to the previous state. A quantity used to determine whether or not a move should be accepted is the change in free energy associated with such a move, δV. The change in energy, δV, is the difference between

the energy of the current state, n, relative to the previous state, m. Considering a pair-potential, $u(r)$, the energy of a certain state is the pair interaction energies between all the particles at that state. Note that with every change, one does not need to calculate the energy of the whole ensemble but simply the relative energy between the displaced particle i and the previous system m compared to the energy of particle i with the rest of the particles in state n. Overall, the change in energy of going from ensemble state m to state n can be written as:

$$\delta V_{m\to n} = \left(\sum_{j=0}^{n} v(r_{ij}^{n}) - \sum_{j=0}^{n} v(r_{ij}^{m}) \right) \tag{25}$$

With δV readily available to compare two different states, the next step is to determine whether or not the new state, consisting of a displaced particle, is favorable. There are two distinct cases depending on what δV is. If the move to the new state decreases the energy of the state $\delta V \leq 0$, then the move is automatically accepted. If the move increases the energy of the system, $\delta V > 0$, then a decision is made to accept the new state with the probability P, with which energetically unfavorable displacements take place in an equilibrium system according to Boltzmann statistics.

In order to accept a new state with only a certain probability, random numbers are generated between 0 and 1 and are compared to an adequate reference probability. In the Metropolis method, the reference probability is the ratio of the Boltzmann factor of the energy difference in transferring from one state to the other. The Boltzmann factor of a state, ρ_m, is defined as: $\rho_m = exp(-\beta V_m)$, where β is the inverse of the thermal energy, $\beta = (k_B T)^{-1}$. Consequently, the Boltzmann factor of going from state m to state n is described as the ratio of probabilities as follows,

$$\frac{\rho_n}{\rho_m} = \frac{e^{(-\beta V_n)}}{e^{(-\beta V_m)}} = \frac{e^{(-\beta V_m)} \cdot e^{(-\beta \delta V_{m\to n})}}{e^{(-\beta V_m)}} = e^{(-\beta \cdot \delta V_{m\to n})} \tag{26}$$

Note that for a energy difference of $\delta v = 0$, the reference probability, $exp(-\beta \delta V_{m\to n})$ is 1 and decreases exponentially with increasing values of $\delta V_{m\to n}$. Considering theory,

larger numbers of $\delta V_{m\to n}$ mean that the move is increasingly more unlikely. Consequently, when generating a random number, ξ, between 0 and 1, the two possibilities are: if the random number falls below the reference probability, $\xi < exp(-\beta\delta V_{m\to n})$, the new state is accepted. Otherwise, if the random number falls above the reference probability, $\xi > exp(-\beta\delta V_{m\to n})$, the move is rejected and we return to the old state.

In an MC simulation, defining equilibrium is not trivial; only equilibrium ensembles should be used to compute a g(r). A measure of equilibrium in MC simulations is achieving a constant ratio between the number of accepted moves relative to the number of rejected moves. The variable that controls this ratio is the maximum allowed displacement distance each particle can travel. Large particle displacements have a high probability of being rejected, due to the higher probability of running into each other's strong repulsions at small inter-particle separations. Therefore, routines include an adjustment mechanism that varies the maximum displacement until a certain, arbitrary ratio of accepted moves to rejected moves is achieved, a measure that means that on average, free energy is not changing with time, in essence the definition of equilibrium.

With moves now readily defined, the simulation consists of repeating many loops of the procedure and generating theoretical dispersion states. After which, the theoretical states can be processed into particle distributions, in this case an appropriate one is the radial distribution function, g(r) with which experimental results can be further compared to.

4.2.2 Monte-Carlo Results

4.2.2.1 Monte-Carlo to compare experiments in Hexane with Span 85

In this study, the method used to convert the g(r) into u(r) is through the Ornstein-Zernike equation with the HNC approximation closure relation. The HNC is, as its name implies, an approximation. Independent studies have shown that the HNC approximation is a good routine for relatively soft potentials [29]. In this study,

the g(r) are "soft" in nature, as observed by gradual increases in the g(r) in Figure 13 rather than hard "steep" rises. Still, in this study, the Monte-Carlo method is used to conclusively make sure the the HNC approximation is appropriate for the experimental measurements performed in this study.

The first set of MC simulations use as input the Screened-Coulomb potentials, with interpolation, obtained from the experimental g(r). The results from the MC method are theoretical g(r) for each of the experiments of particle interactions in nonpolar solutions of Span 85. The resulting g(r)'s from this experiment are shown in Figure 26.

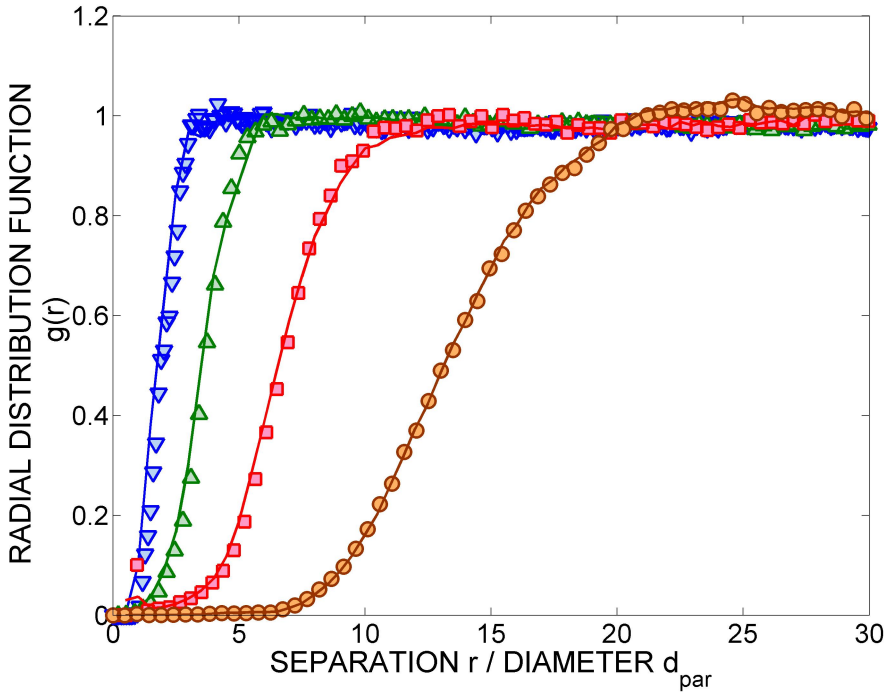

Figure 26: Radial distribution function of experimental data (markers) together with simulation output (lines)

The resulting g(r) curves fit well with the experimental g(r). The simulated g(r) show the same trend as the experimental g(r) and keep the same features. This result suggests that at the the current experimental conditions, at the current particle concentrations in particular, the HNC approximation is an adequate procedure to

Table 4: Number densities of theoretical dispersions used to run Monte-Carlo simulations and test the Hypernetted Chain approximation procedure

Particles per frame	Number density ($*10^{-3}$ nd_{par}^2)
32	1.30
64	2.59
96	3.89
128	5.18
196	7.94

translate a g(r) into a u(r).

4.2.2.2 Hypernetted Chain approximation - concentration dependance

The MC method is used to test the limits of usability of the HNC approximation outlined in the background section with particular focus on the effects of rising particle concentrations. In using the HNC approximation, it is known that it is reliable up to a particle concentration threshold. In order to test the particle density limit, the Metropolis method is applied to recreate the experiments performed on polymer dispersions in Hexane with a 0.7 mM concentration of Span 85. The parameters used in this study are shown in the first row of Table 1.

The particle concentration is the variable in these experiments and is arbitrarily chosen to be 32, 64 and 128 particles per frame. The areal concentrations normalized with the particle diameters, $1.08\mu m$ to be consistent with experiments, are shown in Table 4

In the experimental setup, the frame contained on average 32 particles and in the simulations the concentrations are increased. With a frame dimension kept the same as that in the experimental setup. The results are shown in Figure 27.

The simulated distributions from Figure 27 use as input the same potential; the only variable that has changed is the particle concentration. Visually, however, the

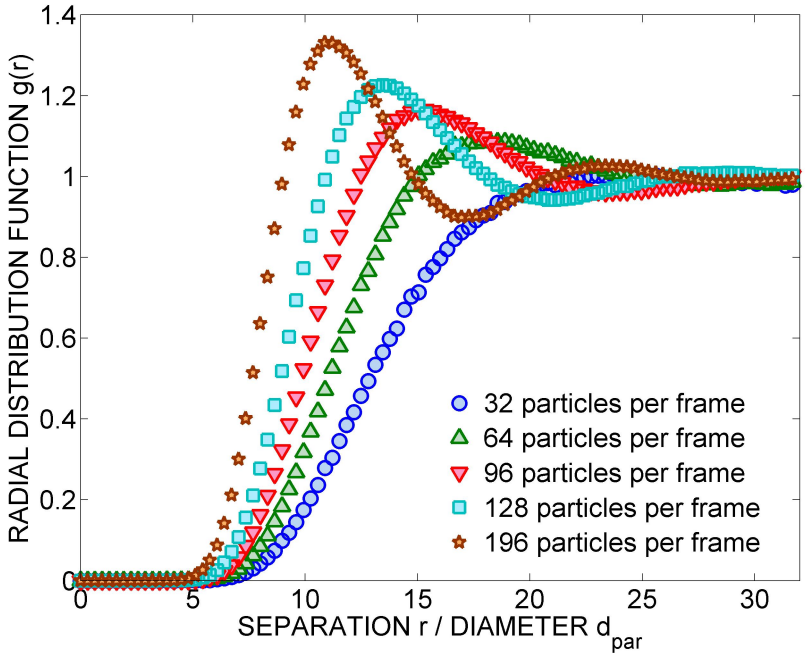

Figure 27: Radial distribution function, g(r) for theoretical states with different particle concentrations and a screened-Coulomb potential based on parameters in the first row of Table 1, in order to test the reliability of the Hypernetted Chain Approximation in 2-D systems

distribution looks substantially different due to the large differences in areal concentrations. The g(r)'s with rising concentrations show the effect of increasing many-body contributions into the radial distribution function. Qualitatively, the g(r) shows beginnings of an arranged structure in the distribution evidenced by the wave-like features that are more pronounced with larger particle concentrations.

An exact conversion of g(r) into a u(r) would find the same u(r), the input potential to the simulation, for all g(r) curves shown in Figure 27. The resulting pair-potentials found by the HNC approximation are shown in Figure 28.

In Figure 28, it can be seen how relatively large particle concentrations can create complications due to the many-body contributions triggered by such high densities. The potential curves, after undergoing the HNC approximation, converge into the same potential, particularly with decreasing particle areal densities. This is intended

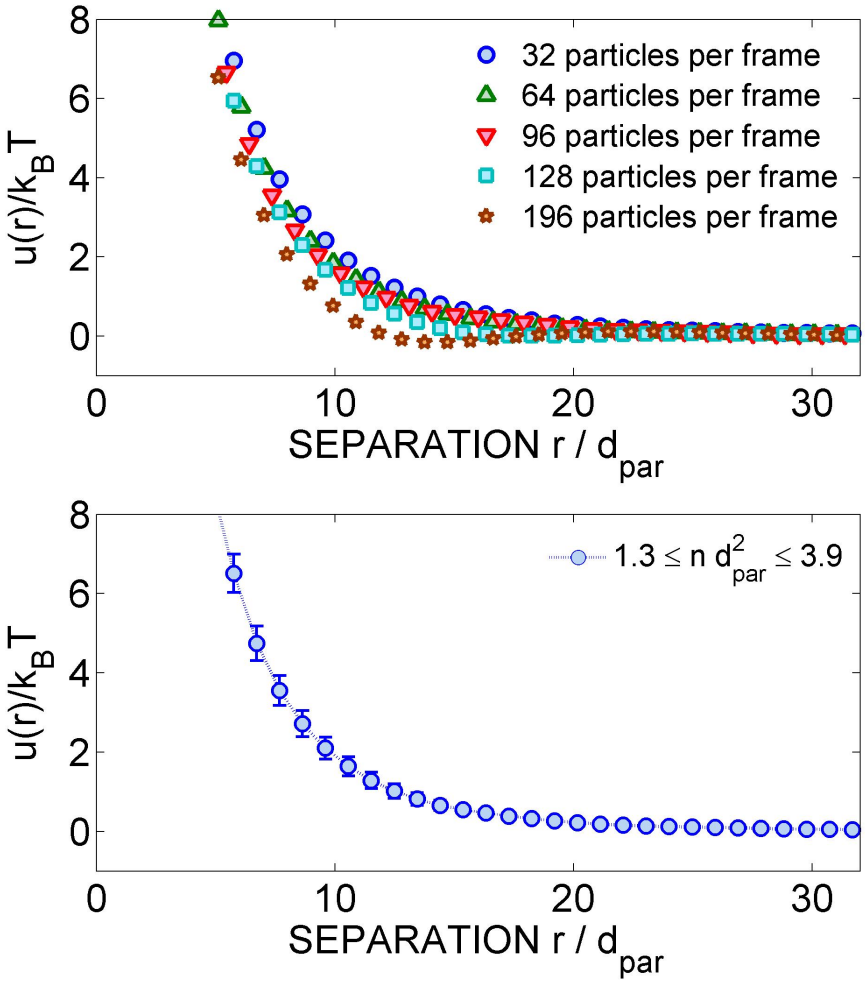

Figure 28: Pair-potentials, u(r), of Monte-Carlo Simulations with varying particle concentrations (top). Pair potential u(r) with standard deviation error bars of the u(r) from simulations using the first three particle concentrations (bottom).

as the input to the Monte-Carlo simulations, the pair-potential, was the same. Yet, do note that the larger the number concentration, the more the deviations in the resulting u(r), however slightly. It seems for instance that the first three particle concentrations, below a value of $\sim 4 \cdot 10^{-3} n d_{par}^2$, converge qualitatively, whereas the last two concentrations show significant deviations from the input. That is, past an areal concentration of $3.89 \cdot 10^{-3} n d_{par}^2$, the HNC approximation should no longer be used to get reliable results.

Experimental results of polymer particle dispersions in nonpolar oils, and the

Monte-Carlo Simulations, are in particle concentrations that fall within the level that give reliable results. The dimensionless concentrations of the experiments in Hexane are in Table 1 and those of the Monte-Carlo simulations are in Table 4. As can be observed by comparing the different number densities used in the experiments, they never go above $nd_{par}^2 = 2.03 \cdot 10^{-3}$ for Span 85 and $nd_{par}^2 = 3.00 \cdot 10^{-3}$ for Span 80 solutions, which is well within a concentration where the HNC approximation translates into accurate potentials.

CHAPTER V

CONCLUSIONS

Recent observations of the electric conductivity and electrophoretic mobility of nonpolar oils with dissolved surfactants have challenged the well-known, intuitive idea that stable charges should not exist in such media. This study utilizes these advancements as a starting point to characterize particle interactions in nonpolar oils, where charges in solution as well as surface charges will be manifested by the interactions.

Through video microscopy experiments and statistical techniques, particle interactions at different concentrations of surfactant, were analyzed in nonpolar systems. The pair potential measurements in this study are the first measurements for polymer particle dispersions in nonpolar oils stabilized by nonionizable surfactants. The interaction is shown to agree with a screened-Coulomb potential at surfactant concentrations both above and below the CMC of the surfactant in the oil phase. Debye lengths, $\kappa^{-1} \sim 0.10$ to $10\mu m$, are found to be orders of magnitude larger than in aqueous systems [36], but similar to the Debye length in nonpolar oils mediated by ionic surfactants [1]. Effective surface charges were calculated to be in the order of 10 to 100 electrons, much lower than for typical aqueous systems. But thanks to the low dielectric constant, these small amounts of surface charge correspond to substantial surface potentials and electrostatic forces easily capable of stabilizing colloidal dispersions.

Monte-Carlo simulations provided a consistency check for the method used in this study to obtain interaction potentials. In particular, simulations test the routines used in this study based on the Ornstein-Zernike integral equation with the hypernetted-chain-approximation closure relation. An areal density limit is obtained,

below which the HNC approximation is able to provide accurate transformation from the radial distribution function g(r) to the pair interaction potential u(r). All experimental particle concentrations fall within this limit; ensuring the trustworthiness of the results.

CHAPTER VI

RECOMMENDATIONS

This study confirmed the presence of ion formation in oils and surface charging in nonpolar media mediated by the use of nonionizable surfactants of the Span family only. A topic adequate for future work is the analyses of particle interactions in nonpolar solutions of nonionizable surfactants not sampled in this study. Surfactants in the Span class where tested in this research, a small subset of the non-ionic surfactants group. Possible classes of nonionizable surfactants include ethylene-glycol-based surfactants or block-copolymers such as PPO-PEO triblock-copolymers known as "Pluronics". Understanding the degree by which many nonionizable surfactants charge a nonpolar fluid would be of great use to determine the detailed mechanism of charging of such systems.

The particles used in this study are made of PMMA polymer. This study showed evidence that surface charging takes place. Furthering the study of surface-charge formation in nonpolar fluids by analyzing different surfaces would provide more evidence useful to characterize the mechanisms by which the surfaces charge. Possible surfaces include other polymers of different chemical nature such as poly-styrene (PS), carbon black particles, or inorganic particles (SiO_2, TiO_2, Fe_2O_3, ...).

Particular experiments to show if a nonionizable surfactant could act as a charge-control agent in a nonpolar phase in contact with an aqueous phase could have great practical impact. Charge formation in nonpolar liquids using surfactants is a relatively young topic, with recent research including evidence of charging using ionic surfactants and only very recently on nonionizable surfactants charging a nonpolar liquid. No research yet exists that reveal what types of surfactants can selectively

charge a nonpolar phase in contact with a charge-friendly water phase. If a nonpolar phase with ionic surfactants (such as AOT) is in contact with a water phase, ionic surfactants initially in the nonpolar phase would partition mostly to the water phase. Such partitioning would render the charge-controlling capabilities of ionizable surfactants to a nonpolar phase inefficient. This is not the case with nonpolar solutions of nonionizable surfactants. Non-ionic surfactants, such as Span-based surfactants in nonpolar liquids in contact with a water phase, will remain mostly in the nonpolar phase. Experiments on oil-borne particles in a 2-liquid phase system could support the novel and counterintuitive notion that nonionic surfactants can sometimes be more efficient charge-control agents than their ionic counterparts.

The nonpolar liquid used in this study is Hexane. Future research on charge formation in other nonpolar liquids, with the mediation of nonionizable surfactants, would improve the understanding of charge formation in other charge-hostile, nonpolar, environments. In low polar solvents, in contrast to nonpolar solvents, weak levels of ion dissociation have been evidenced [18]. Creating systems, based on the results from this study, where charge is formed through disproportionation with nonionizable surfactant micelles combined with low levels of dissociation, could illustrate the relative strength of each charging mechanism in different media.

REFERENCES

[1] M.F. Hsu, E.R. Dufresne, and D.A. Weitz. Charge stabilization in nonpolar solvents. *Langmuir*, 21(11):4881–4887, May 2005.

[2] Pal V. Hemmingsen, Anne Silset, Andreas Hannisdal, and Johan Sjoblom. Emulsions of heavy crude oils. i: Influence of viscosity, temperature, and dilution. *Journal of Dispersion Science and Technology*, 26(5):615, 2005.

[3] Barrett Comiskey, J. D. Albert, Hidekazu Yoshizawa, and Joseph Jacobson. An electrophoretic ink for all-printed reflective electronic displays. *Nature*, 394(6690):253–255, July 1998.

[4] Marc B. Brown, Gary P. Martin, Stuart A. Jones, and Franklin K. Akomeah. Dermal and transdermal drug delivery systems: Current and future prospects. *Drug Delivery*, 13(3):175–187, May 2006.

[5] Pawel Pieranski. Two-Dimensional interfacial colloidal crystals. *Physical Review Letters*, 45(7):569, 1980. Copyright (C) 2010 The American Physical Society; Please report any problems to prola@aps.org.

[6] O. D. Velev, K. Furusawa, and K. Nagayama. Assembly of latex particles by using emulsion droplets as templates. 1. microstructured hollow spheres. *Langmuir*, 12(10):2374–2384, 1996.

[7] Ian D. Morrison. Electrical charges in nonaqueous media. *Colloids and Surfaces A: Physicochemical and Engineering Aspects*, 71(1):1–37, May 1993.

[8] Hans Friedrich Eicke and Vladimir Arnold. Interactions of proton donors with colloidal electrolytes in apolar solvents. *Journal of Colloid and Interface Science*, 46(1):101–110, 1974.

[9] Sunil K. Sainis, Jason W. Merrill, and Eric R. Dufresne. Electrostatic interactions of colloidal particles at vanishing ionic strength. *Langmuir*, 24(23):13334–13337, December 2008.

[10] R. E. Kornbrekke, I. D. Morrison, and T. Oja. Electrophoretic mobility measurements in low conductivity media. *Langmuir*, 8(4):1211–1217, April 1992.

[11] Roland I. Keir, Suparno, and John C. Thomas. Charging behavior in the Silica/Aerosol OT/Decane system. *Langmuir*, 18(5):1463–1465, March 2002.

[12] Wuge H. Briscoe and Roger G. Horn. Direct measurement of surface forces due to charging of solids immersed in a nonpolar liquid. *Langmuir*, 18(10):3945–3956, May 2002.

[13] G. Seth Roberts, Rodrigo Sanchez, Roger Kemp, Tiffany Wood, and Paul Bartlett. Electrostatic charging of nonpolar colloids by reverse micelles. *Langmuir*, 24(13):6530–6541, July 2008.

[14] Filip Strubbe, Alwin R.M. Verschueren, Luc J.M. Schlangen, Filip Beunis, and Kristiaan Neyts. Generation current of charged micelles in nonaqueous liquids: Measurements and simulations. *Journal of Colloid and Interface Science*, 300(1):396–403, August 2006.

[15] Andrei S. Dukhin and Philip J. Goetz. How non-ionic "electrically neutral" surfactants enhance electrical conductivity and ion stability in non-polar liquids. *Journal of Electroanalytical Chemistry*, 588(1):44–50, March 2006.

[16] Qiong Guo, Virendra Singh, and Sven Holger Behrens. Electric charging in nonpolar liquids because of nonionizable surfactants. *Langmuir*, 26(5):3203–3207, March 2010.

[17] Carlos Espinosa, Qiong Guo, and Sven H. Behrens. Particle charging and charge screening in nonpolar dispersions with nonionizable surfactants. *To be submitted.*

[18] Ph. C. Van Der Hoeven and J. Lyklema. Electrostatic stabilization in nonaqueous media. *Advances in Colloid and Interface Science*, 42:205–277, October 1992.

[19] Ayao Kitahara, Tokuko Kobayashi, and Taro Tachibana. Light scattering study of solvent effect on micelle formation of aerosol OT. *The Journal of Physical Chemistry*, 66(2):363–365, February 1962.

[20] J. Lyklema. Principles of the stability of lyophobic colloidal dispersions in nonaqueous media. *Advances in Colloid and Interface Science*, 2(2):67–114, July 1968.

[21] B.V. Derjaguin and L Landau. Colloidal stability of protein-polymer systems: A possible explanation by hydration forces. *Acta Physiocochim USSR*, 14:663, 1941.

[22] W. E. J. Verwey and G Overbeek. Theory of the stability of lyophobic colloids: The interactions of sol particles having an electric double layer. *Elsevier*, 1948.

[23] D. Fennell Evans and Hakan Wennerstrom. *The Colloidal Domain: Where Physics, Chemistry, Biology, and Technology Meet.* Wiley-VCH, 2 edition, February 1999.

[24] John C. Crocker and D.G. Grier. Microscopic measurement of the pair interaction potential of charge-stabilized colloid. *Physical Review Letters*, 73(2):352, 1994.

[25] John C. Crocker and David G. Grier. Methods of digital video microscopy for colloidal studies. *Journal of Colloid and Interface Science*, 179(1):298–310, April 1996.

[26] Bum Jun Park and Eric M. Furst. Optical trapping forces for colloids at the Oil-Water interface. *Langmuir*, 24(23):13383–13392, December 2008.

[27] J. A. Barker and D. Henderson. What is "liquid"? understanding the states of matter. *Reviews of Modern Physics*, 48(4):587, October 1976. Copyright (C) 2010 The American Physical Society; Please report any problems to prola@aps.org.

[28] J. A. Barker and D. Henderson. Theories of liquids. *Annual Review of Physical Chemistry*, 23:439–484, October 1972.

[29] Malgorzata Borowko and Malgorzata Borowko. *Computational Methods in Surface and Colloid Science*. Marcel Dekker, Inc, New York + Basel, 2000.

[30] Sven H. Behrens and David G. Grier. Pair interaction of charged colloidal spheres near a charged wall. *Physical Review E*, 64(5):050401, 2001.

[31] E.M. Chan. Two-dimensional Born-Green-Yvon and other integral equations. *Journal of Physics C: Solid State Physics*, 10:3477, September 1977.

[32] M. Pannek, T. Dunkel, and D. W. Schubert. Effect of a bell-shaped cover in spin coating process on final film thickness. *Materials Research Innovations*, 4(5):340–343, April 2001.

[33] E.W. Flick. *Industrial Solvents Handbook (5th Edition)*. William Andrew Publishing/Noyes, 1998.

[34] Arieh Ben-Naim. *Molecular Theory of Solutions*. Oxford University Press, USA, October 2006.

[35] Sven Holger Behrens, Daniel Iso Christl, Rudi Emmerzael, Peter Schurtenberger, and Michal Borkovec. Charging and aggregation properties of carboxyl latex particles: Experiments versus DLVO theory. *Langmuir*, 16(6):2566–2575, March 2000.

[36] John C. Crocker and D.G. Grier. When like charges attract: The effects of geometrical confinement on Long-Range colloidal interactions. *Physical Review Letters*, 77(9):1897, 1996.

[37] Nicholas Metropolis and S. Ulam. The monte carlo method. *Journal of the American Statistical Association*, 44(247):335–341, September 1949. ArticleType: primary_article / Full publication date: Sep., 1949 / Copyright Â© 1949 American Statistical Association.

[38] M. P. Allen and D. J. Tildesley. *Computer Simulation of Liquids*. Oxford University Press, USA, June 1989.